Mineralogical Magazine (2024), 1–18
doi:10.1180/mgm.2024.20

CAMBRIDGE UNIVERSITY PRESS

Article

Mineralogical zoning of the PGE–Cu–Ni orebodies in the central part of the Oktyabr'sky Deposit, Norilsk District, Russia

Nadezhda D. Tolstykh[1], Nadezhda A. Krivolutskaya[2], Lyudmila S. Canhimbue[3], Bronislav I. Gongalsky[4] and Ivan A. Kuzmin[1]

[1]VS Sobolev Institute of Geology and Mineralogy, SB RAS, Novosibirsk; [2]VI Vernadsky Institute of Geochemistry and Analytical Chemistry, RAS, Moscow; [3]Empress Catherine II Saint Petersburg Mining University, St. Petersburg; and [4]Institute of Geology of Ore Deposits, Petrography, Mineralogy and Geochemistry, RAS, Moscow

Abstract

Mineralogical features of two orebodies, lenses (C-3 and C-4), at the central part of the Oktyabr'sky deposit have been investigated. Multidirectional mineralogical zoning in the northern and southern orebodies is shown, confirming the hypothesis of their formation from various magmatic flows, which have individual features and their own modes of formation. The southern C-3 and northern C-4 orebodies differ in their mineralogical associations: C-3 is characterised by a high-sulfur association of sulfides; and C-4 contains minerals with a sulfur deficit (talnakhite, sugakiite). Variations in Fe and Ni ratios in pentlandite are controlled by the volatility of sulfur during ore crystallisation. Direct crystallisation zoning is observed in the disseminated ores of the C-4 orebody (borehole RT-107), where the fugacity of sulfur (f_{S_2}) increases from bottom to top. In contrast in orebody C-3 (borehole RT-30) f_{S_2} decreases in the same direction. This reverse zoning coincides with the vectors of the evolution of ore systems in various blocks of the Main Ore Body of the Oktyabr'sky deposit. The difference in typomorphic features of disseminated ores of the southern and northern orebodies is confirmed by differences in the associations of platinum-group element minerals (PGMs). Disseminated ores in picritic gabbro-dolerites and massive pyrrhotite ores in the exocontact of the intrusion within the southern orebody differ in the specialisation of PGMs: the former is characterised by minerals of the Pd–Bi–Sb–Te system, the latter by only Pt minerals. The similarity of these types of ores lies in the similar reverse mineralogical and geochemical zoning from top to bottom along the sections, caused by the evolution of the sulfide melt in this direction. The formation of reverse zoning of disseminated ores (zones of 'marginal reversion') is probably due to the action of a mechanism of repeated influx of a melt of an increasingly primitive composition into the upper parts of the crystallising flow. Unidirectional trends in massive and disseminated ores are more likely to be due to the action of the same type of mechanism.

Keywords: PGE–Cu–Ni ore; geochemistry–mineralogical zoning; evolution of sulfide melt; northern and southern orebodies; Oktyabr'sky deposit

(Received 23 October 2023; accepted 12 March 2024; Accepted Manuscript published online: 15 April 2024; Associate Editor: Daniel Atencio)

Introduction

The Oktyabr'sky deposit plays an important role in solving genetic problems of the unique platinum–copper–nickel ores in the Norilsk region, in addition, it is the largest deposit related to the Kharaelakh layered intrusion, located in the south of the Kharaelakh trough (Fig. 1).

The Oktyabr'sky deposit is a collection of at least 15 massive (and overlying disseminated) orebodies or lenses (Dyuzhikov *et al.*, 1992; Stekhin, 1994; Torgashin, 1994). They are variously located close to each other, or separated spatially as in the C-3 and C-4 orebodies, however these orebodies (or lenses) as a whole make up the Oktyabr'sky deposit. A huge amount of analytical data has been obtained for the Main Ore Body – a lode of massive sulfide ore, 4 × 2 km with thickness up to 50 m). The genesis of the Main Ore Body has been the subject of intensive discussions for several decades (Genkin, 1968; Dodin and Batuev 1971; Distler *et al.*, 1975, 1988, 1996; Genkin *et al.*, 1981; Zientek and Likhachev, 1992; Likhachev, 1994, 2006; Naldrett *et al.*, 1994, 1995, 1996; Naldrett, 2004; Sluzhenikin, 2011; Krivolutskaya *et al.*, 2018, and many others).

The Main Ore Body has mineralogical zoning: mooihoekite ($Cu_9Fe_9S_{16}$) – talnakhite ($Cu_{18}(Fe, Ni)_{18}S_{32}$) – chalcopyrite ($CuFeS_2$) ore transforms into cubanite ($CuFe_2S_3$) ore, and then into pyrrhotite ($Fe_{1-x}S$) ore from the centre to the flank (Dyuzhikov *et al.*, 1992; Torgashhin, 1994; Lul'ko *et al.*, 1994; Naldrett *et al.*, 1995; Valetov *et al.*, 2000; Gorbachev, 2006; Dodin *et al.*, 2009). That is, the iron content in the ores increases in this direction. The origin of this 'reverse' zoning is one of the main genetic questions. The Main Ore Body cannot be considered as a single lode crystallised in a closed system, as from the point of view of crystallisation differentiation the more fractionated parts of orebodies enriched in Cu and platinum-group elements (PGE), which are incompatible with monosulfide solid solution (Mss), should be located on the periphery (Distler *et al.*, 1975;

Corresponding author: Nadezhda D. Tolstykh; Email: tolst@igm.nsc.ru
Cite this article: Tolstykh N.D., Krivolutskaya N.A., Canhimbue L.S., Gongalsky B.I. and Kuzmin I.A. (2024) Mineralogical zoning of the PGE–Cu–Ni orebodies in the central part of the Oktyabr'sky Deposit, Norilsk District, Russia. *Mineralogical Magazine* 1–18. https://doi.org/10.1180/mgm.2024.20

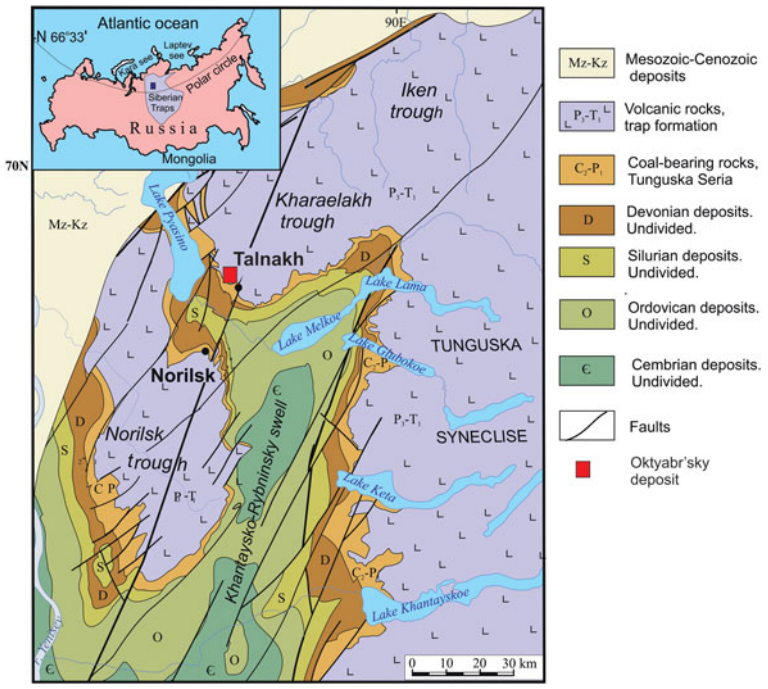

Figure 1. Geological schema of the Noril'sk area (based on Geological map 1:200000, from Strunin, 1994).

Zientek *et al.*, 1994; Barnes *et al.*, 2011). Experimental (Likhachev and Kukoev, 1973; Sinyakova *et al.*, 2019) and modelling (Distler, 1975; Kalugin and Latypov, 2009) work have confirmed that direct zoning is formed during fractional crystallisation when the more fractionated constituents of sulfide melts are distilled to the periphery.

The horizontal zoning of the Oktyabr'sky deposit is very complex, and reflects the interaction of different-scale genetic factors such as: the separation of the sulfide melt in the intermediate chamber into Fe-rich and Cu-rich fractions that can then be introduced separately (Gorbachev and Nekrasov, 2004; Gorbachev, 2006; Likhachev, 2006); various directions of the flows (streams) of sulfide melts and the pattern of these flows laterally (Stekhin, 1994); a single-act or the pulsating nature of their introduction; and the fractionation of the sulfide melt during the flow differentiation, with the distillation of its more cuprous derivatives into the frontal parts.

In comparison, the vertical zoning of orebodies depend on: the degree of fractionation of the sulfide melt *in situ* and the behaviour of elements that are compatible and incompatible with Mss during its crystallisation; possible degassing of the sulfide melt (Godlevsky, 1968; Gorbachev, 2006) when surface capillary forces are dominant over gravity (Barnes *et al.*, 2019); and the pulsation mode of incoming melts (Latypov *et al.*, 2007, 2011; Egorova and Latypov, 2013).

If we consider the Oktyabr'sky deposit on a large scale, then the influence of the Norilsk-Kharaelakh fault is important for the overall configuration of ore zoning (Stekhin, 1994). The zoning of ores is associated primarily with the action of a series of linear flows directed from the fault that provides supply channels for intrusive material (Fig. 2). Each flow is characterised by the distribution of pyrrhotite ores in the root parts and near the fault, and more cuprous ores forming halos around the pyrrhotite ores (Kunilov, 1994). The MOB is composed of at least two ore lenses corresponding to the different flows of sulfide melt – pyrrhotite is predominant in the first lens, and a mooihoekite–cubanite–chalcopyrite assemblage is common in the second lens (Torgashin, 1994; Kalugin and Latypov, 2010, 2012). The vertical zoning of cuprous and pyrrhotite ores are the opposite, i.e. the contents of Cu, PGE and Au increase from the bottom to the top (direct zoning) in cuprous lenses, whereas the contents increase from the top to the bottom in pyrrhotite lenses – reverse zoning (Fig. 3) (Torgashin, 1994; Gorbachev, 2006; Kalugin and Latypov, 2010, 2012).

Lenses C-3 and C-4 belong to different flows of silicate magma and sulfide melt (Fig. 2): the northern lens C-4 belongs to a

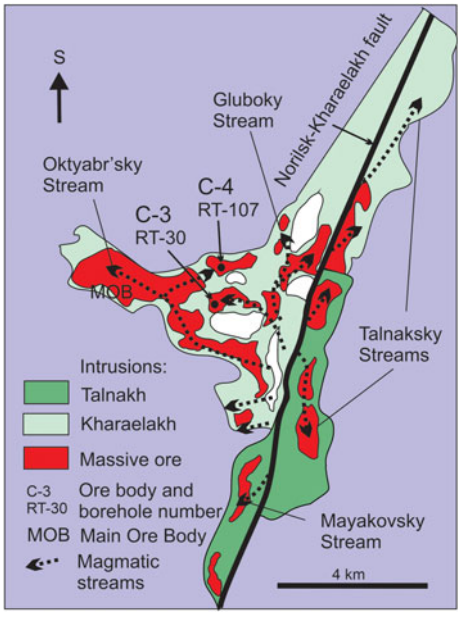

Figure 2. Plan view of the Talnakh ore cluster with contours of massive ore and flow directions of fractionating ore magma. Redrawn from Stekhin (1994).

https://doi.org/10.1180/mgm.2024.20 Published online by Cambridge University Press

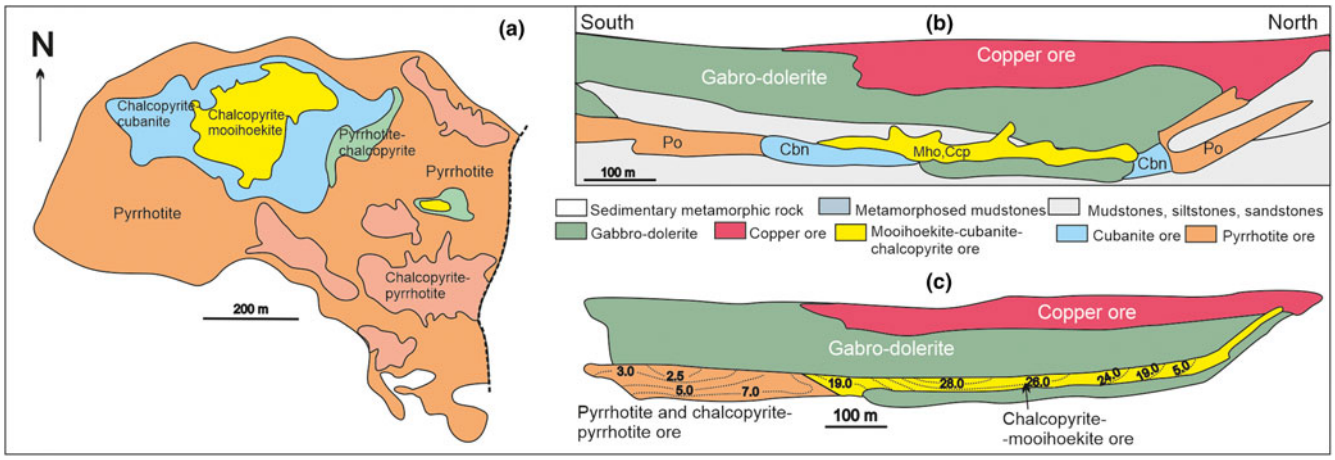

Figure 3. Schematic map of the massive ores (a), and sections (b,c) of the Oktyabr'sky deposit by Torgashin (1994) (redrawn with some changes). Details: (b) large scale lateral zoning of massive ores from Cu-rich in the centre of the Main Ore Body to pyrrhotite-rich on the periphery; (c) vertical zoning expressed as a decrease in Cu concentrations (reverse zoning) up the section of the pyrrhotite ore and an increase (direct zoning) in the Cu-rich ore (Torgashin, 1994).

branch of the extended 'Oktyabr'sky flow', and the southern lens C-3 belongs to another flow (unnamed), extending northwest from the regional fault (Stekhin, 1994). Their study is very important for understanding the conditions for the formation of the deposit as a whole (Krivolutskaya, 2014; Krivolutskaya *et al.*, 2019; 2021).

We present new mineralogical data from boreholes on two orebodies in the central part of the Oktyabr'sky deposit, including both massive and disseminated ores located at the bottom of the Kharaelakh intrusion: C-3 in the south and C-4 in the north of this area (Fig. 2). These boreholes are characterised by different mineral associations of both sulfides and platinum-group minerals (PGM). This work has two objectives: (1) to demonstrate the mineralogical differences and similarity between disseminated and massive ores; (2) to show typomorphic features of disseminated ores in picritic gabbro-dolerite for C-3 (RT-30 borehole) and C-4 (RT-107 borehole) orebodies to verify the difference in their genesis.

Brief geology of the Norilsk district

The geology of the Talnakh ore cluster and the Oktyabr'sky deposit, related to the Kharaelakh intrusion is described in many publications (for example: Zolotukhin, 1964; Zolotukhin *et al.*, 1975; Dyuzhikov *et al.*, 1992; Torgashin, 1994; Stekhin, 1994; Likhachev, 1996; Turovtsev, 2002). This intrusion belongs to the Norilsk intrusive complex (Dyuzhikov *et al.*, 1992) and is located within the carbonate–sulfate–terrigenous rocks, mostly, at the boundary of the Razvedochninsky and Kureysky Formations, and partially in the Manturovsky Formation (western flanks). The Devonian sediments are overlapped by the coal-bearing Tunguska series and P_3-T_1 tuff-lavas of the Ivakinsky, Syverminsky, Gudchikhinsky, Khakanchansky, Nadezhdinsky, Morongovsky and Mokulaevsky formations (Figs 1, 4). The Kharaelakh intrusion, like other intrusions of the Norilsk complex, is composed of a differentiated series of gabbro-dolerites, with varying amounts of olivine that decrease from bottom to top

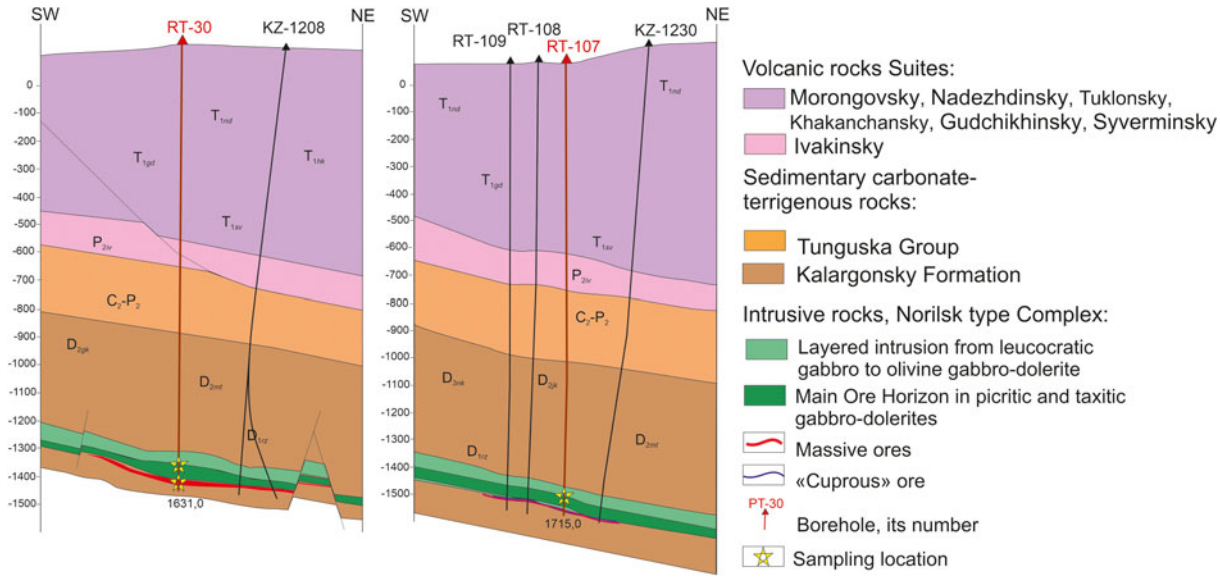

Figure 4. Sections of the intrusion showing the position of boreholes with the studied ores of the Oktyabr'sky deposit according to 'Norilskgeologiya' LLC, Norilsk Nickel company.

https://doi.org/10.1180/mgm.2024.20 Published online by Cambridge University Press

(Fig. 4), i.e. in the order: contact, taxitic, picritic, olivine, olivine-bearing, olivine-free; leucogabbro, gabbro-diorite, ferrogabbro, upper taxitic, and then upper picritic gabbro-dolerites form the upper intrusive zone. Hereinafter, the nomenclature of rocks adopted in the legend to the 1: 200,000 scale Geological Map is used (Strunin, 1994).

The picritic gabbro-dolerite are considered a cumulative part of the main layered series (Likhachev, 1996; Distler *et al.*, 1999). Massive ores of various thicknesses are located at the contact of the intrusion with the host rocks. They are separated from the intrusion by a horizon of host hornfelses, with thicknesses reaching, for example, 19 m in borehole RT-30 and only 3 m in RT-107 (Fig. 5).

Methods of analysis

The analyses of sulfides and minerals of the platinum-group elements and high-resolution electronic imaging were performed at the Analytical Center for Multi-Element and Isotope Research of the IGM of SB RAS, Novosibirsk (N.S. Karmanov) by X-ray spectral methods using microanalysers (SEM-EDS) MIRA 3 LMU (Tescan Ltd) with an INCA Energy 450+ XMax 50+ and Inca Wave 500 microanalysis system (Oxford Instruments Ltd). Analytical conditions were: beam size ~2 μm and accelerating voltage 20 kV; beam current 30–50 nA over the sample surface; and beam diameter ~1 μm. The measurement duration was 20 s for each analytical line. The following standards were used: FeS_2 (S), $PtAs_2$ (As), HgTe (Te), metallic Zn, Co, Ni, Cu, Pt, Pd, Au, Ag, Sn, Sb, etc. The limit of detection for the majority of the elements was 0.2–0.3% (3 sigma criterion). The correction of matrix effects was performed using the *XPP* software algorithm. The accuracy and reproducibility of the analytical procedure were evaluated by comparing the results of EDS and WDS analysis on sulfides (pyrrhotite, pentlandite and chalcopyrite) in the RT-107 borehole, identifying the macrocomponents (Fe, Ni, Cu, Co), and confirmation using special tests (Korolyuk *et al.*, 2009). We also carried out a comparison of EDS and WDS analysis of pentlandite from samples of picritic gabbro-dolerites in both boreholes, resulting in convincing compositions of pentlandite obtained by the different methods. Therefore the EDS results were used; all other minerals were analysed by X-ray spectral methods on microanalysers (SEM-EDS) MIRA 3 LMU.

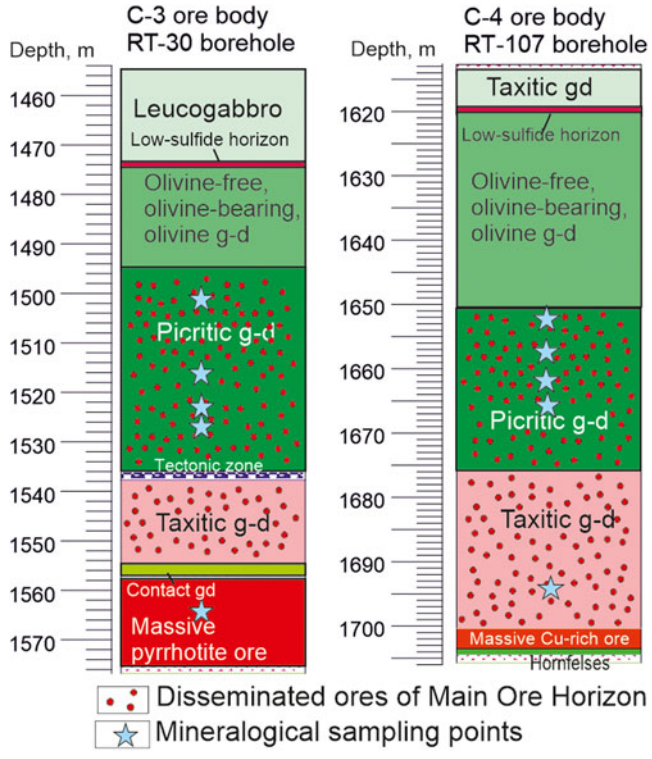

Figure 5. Schematic columns of boreholes RT-30 and RT-107 with sampling points.

Results

General characteristics of the sulfide ores

Sulfide associations and PGMs were investigated in samples of disseminated ores from picritic and taxitic gabbro-dolerites above the northern body C-4 and southern body C-3 (in boreholes RT-107 and RT-30, correspondingly). Picritic gabbro-dolerites of the Oktyabr'sky deposit, in addition to all other deposits of the Norilsk complex, are represented by fine- to medium-grained massive rocks consisting of (wt.%): olivine (50–80); clinopyroxene (20–30); plagioclase (20–40); and orthopyroxene (~5). Sulfides in the picritic gabbro-dolerite of both boreholes are composed of drops and small segregations of chalcopyrite–pentlandite–cubanite–pyrrhotite composition (Fig. 6a–d). Massive ores of the southern C-3 orebody are essentially pyrrhotite in composition. Pyrrhotite commonly occurs as intergrowths of crystals of various modifications (troilite and hexagonal), and can be found with second generation exsolution inclusions of pentlandite (Fig. 6h). Chalcopyrite grains of various sizes are surrounded by pentlandite rims of the first generation (Fig. 6h,i).

The sulfur concentration in the disseminated ores does not exceed 6 wt.% in the picritic gabbro-dolerite and 0.5 wt.% in taxitic rocks; PGE contents in both rocks are in single percent levels; and Pd prevails over Pt. The sulfur concentration in massive ore varies between 41.8–47.8 wt.% and the (Pd + Pd) concentrations reach 30 ppm.

Sulfide associations.

We have analysed disseminated sulfides in the following samples taken from different levels of the picritic gabbro-dolerites, i.e. in RT-30: at 1501.2, 1516, 1523 and 1527, and in RT-107: at 1652, 1657.2 and 1665.4 m (Fig. 5). They are composed mainly of pyrrhotite (Po) or troilite (Tr), chalcopyrite (Ccp) and pentlandite (Pn) (Table 1).

The iron–nickel ratio in pentlandite varies significantly in the picritic gabbro-dolerite in the sections: both ferruginous and nickel-rich varieties are present however Fe-rich pentlandite predominates (Fig. 7a,b), including Co up to 3.47 wt.% (Table 1, No. 31). The most Fe-rich compositions of pentlandite occur at a deeper horizon (1665.4 m) of picritic ore over the northern orebody C-4, and the content of Ni in pentlandite, as well as S in pyrrhotite, increases up the section towards the 1652 m horizon (Table 1, Fig. 7a). Whereas the opposite direction of these changes occurs in the disseminated ore over the southern orebody: Fe-rich Po and S-poor Po (troilite) are located in the upper part of the picritic layer (1501.2 m), and the most enriched in nickel – at a depth (1527 m) (Table 1, Fig. 7b).

A very important difference between the northern and southern disseminated ores is that the former (in borehole RT-107)

https://doi.org/10.1180/mgm.2024.20 Published online by Cambridge University Press

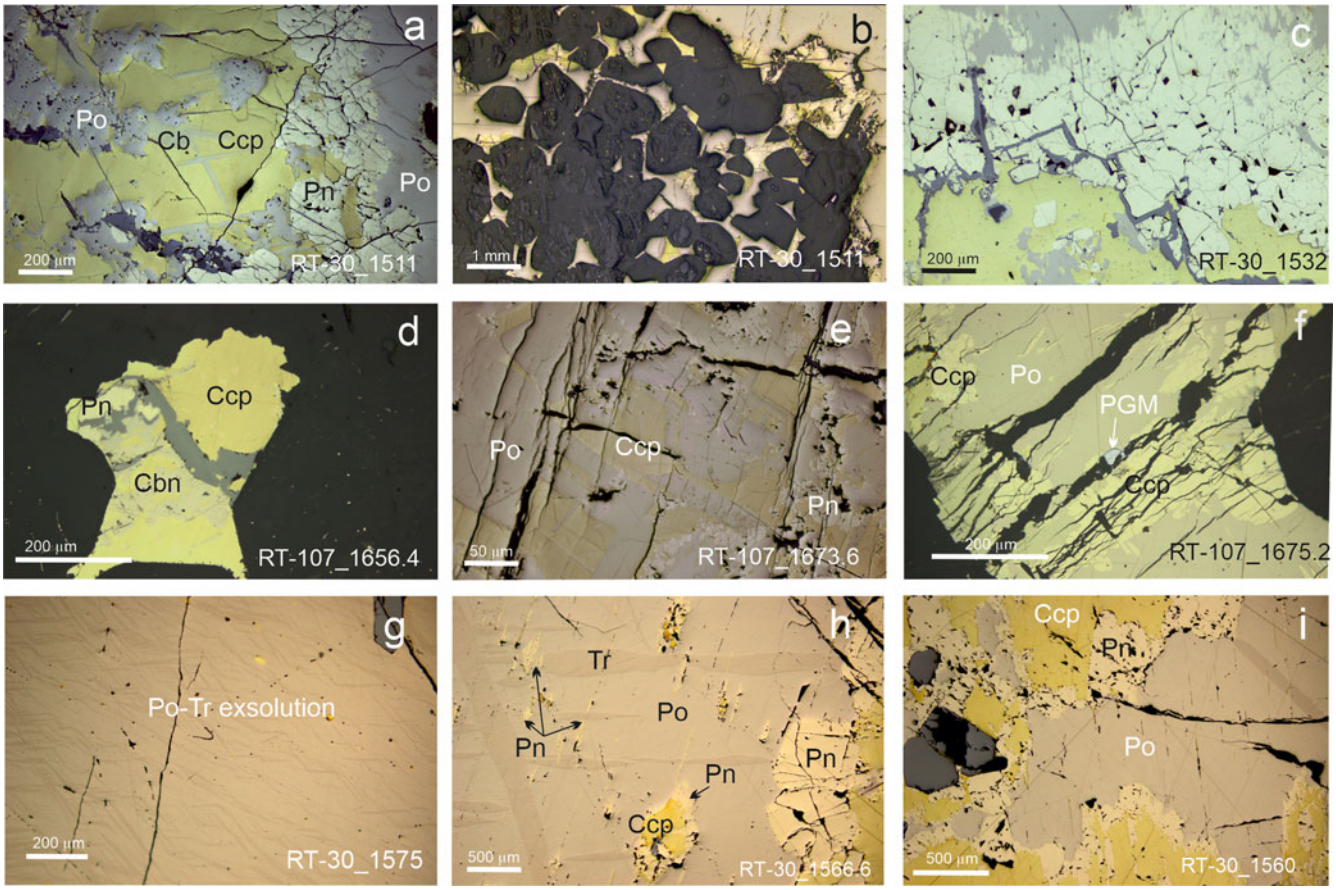

Figure 6. Photomicrograph in reflected light of various types of ores from the southern C-3 (a–c, g–i) and northern C-4 (d–f) orebodies. Details: (a–f) sulfides from disseminated ore in picritic gabbro-dolerite; (g–i) – sulfides from massive ore. Po – pyrrhotite, Ccp – chalcopyrite, Cbn – cubanite, Pn – pentlandite, Mag – magnetite, Tro – troilite, Sil – silicate minerals, PGM – platinum-group minerals.

contains sugakiite $Cu(Fe,Ni)_8S_8$ (Fig. 7a) and sulfides deficient in sulfur of the chalcopyrite group (approaching talnakhite in composition) (Fig. 7d), whereas the latter ores (RT-30) comprise only stochiometric chalcopyrite (tetragonal). Sugakiite, a rare mineral, occurs as granular (60–120 μm) grains intergrown with pyrrhotite at the bottom part of the picritic horizon (1665.4 m). The concentration of copper in sugakiite varies from 0.48–0.90 wt.% (Table 1, Nos. 25–28, Fig 7a) and is similar to that of the first discovery described in Hokkaido, Japan (Kitakaze, 2008).

Disseminated ore in the taxitic gabbro-dolerite (RT-107_1698) is represented by monoclinic pyrrhotite, chalcopyrite, cubanite and pentlandite. In detail, Ag-rich pentlandite (0.40–0.56 apfu Ag) and argentopentlandite (0.98–1.02 apfu Ag)], with the Ag concentration in the latter reaching 13.16 wt.%. (Table 1, 56–61), and Fe significantly prevailing over Ni (Table 1, Fig. 7c). Argentopentlandite grains (~100 μm) are included in the chalcopyrite matrix in association with fine Ag-free pentlandite grains framing this chalcopyrite (Table 1, Fig. 8a,b,f).

The massive ore of the southern orebody (RT-30_1566) is characterised by a predominance of pyrrhotite over other sulfides. Pentlandite occurs in two generations: Pn_1 as rims around chalcopyrite segregations, and Pn_2 as thin lamellae – exsolution inclusions in a pyrrhotite matrix. Pentlandite contains ubiquitous Ni, up to 1 wt.%, and Co from 1.42 to 1.80 wt.%. Compositions of pentlandite vary within small limits and belong to both Fe-rich and Ni-rich varieties (Fig. 7c). Compositions intermediate between cubanite and chalcopyrite are, possibly, a fine exsolution texture between these minerals (Fig. 7d).

Association of minerals of the Platinum Group Elements (PGM)

Disseminated ore in the picritic gabbro-dolerite of the southern C-3 orebody (RT-30_1527) contains the following PGMs: sperrylite $PtAs_2$ grains (30–50 μm) intergrown with chalcopyrite and pentlandite (Fig. 9a,c,i); Te- and Sb-bearing sobolevskite Pd(Bi, Te, Sb) (Fig. 9b,f,g); sopcheite $Ag_4Pd_3Te_4$ as a small (2 μm) inclusion in pentlandite (Fig. 9e); stibiopalladinite Pd_5Sb_2 intergrown with sobolevskite and stannopalladinite Pd_5Sn_2Cu (Fig. 9g,h); and single grains of Au–Ag alloys (Fig. 9d). Stannopalladinite from the southern orebody contains Pt up to 7.52 wt.%, sometimes Sb ~2 wt.%, and corresponds to the formula $(Pd,Pt)_5(Sn, Sb)_2Cu$ (Fig. 10a). Sperrylite and stibiopalladinite correspond to their stoichiometric $PtAs_2$ and Pd_5Sb_2 formulas, whereas sobolevskite Pd(Bi, Te, Sb) forms solid solutions with kotulskite up to 0.38 apfu Te and sudburyite up to 0.09 apfu Sb (Table 2).

The PGM association in disseminated ore in the picritic gabbro-dolerite of the northern C-4 orebody (PT-107) differs from those described above and includes niggliite (PtSn) with gold dissemination (Fig. 11a) in the upper part of the horizon; atokite–rustenburgite solid solutions that dominate in the lower part of this horizon (Fig. 11f,i); paolovite (Pd_2Sn), sometimes as a fine exsolution texture with sobolevskite (Fig. 11h) and minerals intermediate in composition between taimyrite and cabriite (Fig. 10a). Sperrylite is a

https://doi.org/10.1180/mgm.2024.20 Published online by Cambridge University Press

Table 1. Representative compositions of sulfides from boreholes RT-30 (orebody C-3) and RT-107 (orebody C-4) of the Oktyabr'sky deposit.

No.	Sample, depth	Fe	Co	Ni	Cu	Ag	S	Sum	Formula
	Disseminated ores in picritic gabbro-dolerite								
1	PT-107_1657.2	60.74					38.06	98.8	$Fe_{0.96}S_{1.04}$
2	PT-107_1657.2	60.61					37.71	98.32	$Fe_{0.96}S_{1.04}$
3	PT-107_1657.2	61.24					37.80	99.04	$Fe_{0.96}S_{1.04}$
4	PT-107_1665.4	58.41		4.01			35.61	99.04	$(Fe_{0.94}Ni_{0.06})_{1.00}S_{1.00}$
5	PT-107_1665.4	57.82	1.44	3.93			36.16	99.35	$(Fe_{0.92}Ni_{0.06}Co_{0.02})_{1.00}S_{1.00}$
6	PT-107_1665.4	58.80		3.88			35.46	99.17	$(Fe_{0.95}Ni_{0.06})_{1.01}S_{0.99}$
7	PT-30_1501.2	63.20					36.25	99.87	$Fe_{1.00}S_{1.00}$
8	PT-30_1501.2	62.80					35.71	99.26	$Fe_{1.00}S_{1.00}$
9	PT-30_1501.2	62.62					35.85	99.17	$Fe_{1.00}S_{1.00}$
10	PT-30_1516	60.68		0.47			37.69	98.84	$(Fe_{0.96}Ni_{0.01})_{0.97}S_{1.04}$
11	PT-30_1516	61.64	0.36	0.34			37.97	100.31	$(Fe_{0.96}Co_{0.01}Ni_{0.01})_{0.98}S_{1.03}$
12	PT-30_1516	61.04					37.36	98.69	$Fe_{0.97}S_{1.03}$
13	PT-30_1523	60.63		0.64			38.48	99.75	$(Fe_{0.95}Ni_{0.01})_{0.96}S_{1.05}$
14	PT-30_1523	60.8		0.63			38.57	100.0	$(Fe_{0.95}Ni_{0.01})_{0.96}S_{1.04}$
15	PT-107_1652	29.24	1.53	36.16			32.83	99.76	$(Ni_{4.78}Fe_{4.07}Co_{0.20})_{9.05}S_{7.95}$
16	PT-107_1652	29.38	1.56	36.12			33.07	100.13	$(Ni_{4.76}Fe_{4.07}Co_{0.20})_{9.03}S_{7.97}$
17	PT-107_1652	29.16	1.43	35.68			32.95	99.22	$(Ni_{4.74}Fe_{4.07}Co_{0.19})_{9.00}S_{8.01}$
18	PT-107_1657.2	35.28	0.69	30.64			33.16	99.77	$(Fe_{4.88}Ni_{4.03}Co_{0.09})_{9.01}S_{7.99}$
19	PT-107_1657.2	35.04	0.80	30.48			33.15	98.67	$(Fe_{4.86}Ni_{4.02}\ Co_{0.11})_{8.99}S_{8.01}$
20	PT-107_1657.2	35.27	0.87	30.32			33.24	98.83	$(Fe_{4.88}Ni_{3.99}\ Co_{0.09})_{8.99}S_{8.01}$
21	PT-107_1665.4	39.54	2.00	24.92			33.17	99.63	$(Fe_{5.47}Ni_{3.28}Co_{0.26})_{9.01}S_{7.99}$
22	PT-107_1665.4	39.5	2.01	25.04			33.08	99.63	$(Fe_{5.47}Ni_{3.30}Co_{0.26})_{9.03}S_{7.97}$
23	PT-107_1665.4	39.16	2.06	25.02			32.65	98.89	$(Fe_{5.47}Ni_{3.32}Co_{0.27})_{9.06}S_{7.94}$
24	PT-107_1665.4	39.20	2.19	25.32			33.11	99.82	$(Fe_{5.42}Ni_{3.33}Co_{0.29})_{9.04}S_{7.97}$
25	PT-107_1665.4	41.70		20.44	3.98		33.32	99.44	$(Fe_{5.78}Ni_{2.69}Cu_{0.48})_{8.95}S_{8.04}$
26	PT-107_1665.4	42.86		16.58	6.89		32.66	98.99	$(Fe_{5.99}Ni_{2.21}Cu_{0.85})_{9.05}S_{7.95}$
27	PT-107_1665.4	43.11		16.16	7.37		32.93	99.57	$(Fe_{5.99}Ni_{2.14}Cu_{0.90})_{9.03}S_{7.97}$
28	PT-107_1665.4	43.38		16.61	6.31		33.08	99.38	$(Fe_{6.03}Ni_{2.20}Cu_{0.77})_{9.00}S_{8.01}$
29	PT-30_1516	32.79	1.84	32.26			32.98	99.87	$(Fe_{5.54}Ni_{4.25}Co_{0.24})_{9.043}S_{7.96}$
30	PT-30_1516	34.07	0.29	31.48			33.05	98.6	$(Fe_{4.75}Ni_{4.18}Co_{0.04})_{8.97}S_{8.03}$
31	PT-30_1516	32.77	3.47	27.99			33.68	97.91	$(Fe_{4.59}Ni_{3.73}Co_{0.46})_{8.78}S_{8.22}$
32	PT-30_1501.2	40.95	0.42	23.73			32.5	97.18	$(Fe_{5.78}Ni_{3.18}Co_{0.06})_{9.02}S_{7.98}$
33	PT-30_1501.2	39.83	0.75	24.81			33.41	98.05	$(Fe_{5.53}Ni_{3.28}\ Co_{0.10})_{8.91}S_{8.09}$
34	PT-30_1501.2	39.58	0.70	24.68			32.98	97.24	$(Fe_{5.55}Ni_{3.29}Co_{0.09})_{8.94}S_{8.06}$
35	PT-30_1523	32.84	1.89	32.88			32.1	97.82	$(Fe_{4.58}Ni_{4.37}Co_{0.25})_{9.20}S_{7.80}$
36	PT-30_1523	31.64	1.13	32.66			33.53	97.83	$(Fe_{4.40}Ni_{4.32}Co_{0.15})_{8.87}S_{8.13}$
37	PT-30_1527	29.52	2.07	34.80			32.94	99.33	$(Ni_{4.62}Fe_{4.11}Co_{0.27})_{9.00}S_{8.00}$
38	PT-30_1527	29.41	1.76	34.70			32.46	98.33	$(Ni_{4.65}Fe_{4.14}Co_{0.24})_{9.03}S_{7.97}$
39	PT-30_1527	32.43	0.48	32.10			32.18	97.19	$(Fe_{4.61}Ni_{4.35}Co_{0.06})_{9.02}S_{7.98}$
40	PT-107_1652	30.34			33.57		34.36	98.27	$Cu_{0.99}Fe_{1.01}S_{2.00}$
41	PT-30_1501.2	33.12			31.51		33.72	98.35	$Cu_{0.93}Fe_{1.11}S_{1.97}$
42	PT-30_1501.2	34.17			29.68		34.55	98.4	$Cu_{0.87}Fe_{1.13}S_{2.00}$
43	PT-30_1516	30.89			33.96		34.46	99.31	$Cu_{0.99}Fe_{1.02}S_{1.99}$
44	PT-30_1516	30.89			33.21		34.3	98.4	$Cu_{0.97}Fe_{1.03}S_{1.99}$
45	PT-30_1523	29.84			33.09		34.34	97.27	$Cu_{0.98}Fe_{1.01}S_{2.02}$
46	PT-30_1523	30.43			33.33		34.24	98.00	$Cu_{0.98}Fe_{1.02}S_{2.00}$
47	PT-107_1665.4	33.05			30.62		34.12	97.79	$Fe_{1.66}Cu_{1.35}S_{2.99}$
48	PT-107_1665.4	32.74			31.12		34.49	98.35	$Fe_{1.66}Cu_{1.30}S_{3.04}$
	Disseminated ores in taxitic gabbro-dolerite								
49	PT-107_1698	61.54					37.94	99.48	$Fe_{0.96}S_{1.04}$
50	PT-107_1698	61.22		0.56			37.92	99.70	$(Fe_{0.96}Ni_{0.01})_{0.97}S_{1.03}$
51	PT-107_1698	60.51					38.59	99.10	$Fe_{0.95}S_{1.05}$
52	PT-107_1698	59.98					38.71	98.69	$Fe_{0.94}S_{1.06}$
53	PT-107_1698	32.62	1.15	33.34			32.85	99.96	$(Fe_{4.52}Ni_{4.40}Co_{0.15})_{9.07}S_{7.93}$
54	PT-107_1698	32.79	1.23	33.26			33.06	100.34	$(Fe_{4.53}Ni_{4.37}Co_{0.16})_{9.06}S_{7.95}$
55	PT-107_1698	37.75		18.90		13.16	31.39	101.20	$Ag_{0.99}(Fe_{5.47}Ni_{2.61})_{8.08}S_{7.93}$
56	PT-107_1698*	33.23		34.25			33.89	101.37	$(Fe_{4.52}Ni_{4.44})_{8.96}S_{8.04}$
57	PT-107_1698*	37.22		18.89		12.92	30.80	99.83	$Ag_{0.98}(Fe_{5.48}Ni_{2.64})_{8.12}S_{7.89}$
58	PT-107_1698	37.22		18.83		12.86	31.03	99.94	$Ag_{0.98}(Fe_{5.46}Ni_{2.63})_{8.09}S_{7.93}$
59	PT-107_1698	36.05		18.26		13.05	29.97	97.33	$Ag_{1.02}(Fe_{5.45}Ni_{2.63})_{8.08}S_{7.90}$
60	PT-107_1698	35.95		24.61		7.50	31.93	99.99	$(Fe_{5.14}Ni_{3.65}Ag_{0.56})_{9.05}S_{7.95}$
61	PT-107_1698	33.16	0.98	22.46		5.64	37.19	99.43	$(Fe_{4.58}Ni_{2.95}Ag_{0.40}Co_{0.13})_{8.06}S_{8.94}$
62	PT-107_1698	31.08			34.37		34.35	99.80	$Cu_{1.00}Fe_{1.03}S_{1.98}$
63	PT-107_1698*	30.93			34.26		34.26	99.45	$Cu_{1.00}Fe_{1.02}S_{1.98}$
64	PT-107_1698	30.93			34.26		34.26	99.45	$Cu_{1.00}Fe_{1.02}S_{1.98}$
65	PT-107_1698	35.08	0.11		30.10		35.08	100.37	$Cu_{1.29}(Fe_{1.71}Co_{0.01})_{1.72}S_{2.99}$
66	PT-107_1698	35.72	0.09	0.10	29.65		34.55	100.11	$Fe_{1.75}Cu_{1.28}S_{2.96}$
	Massive ore								
67	PT-30_1566	60.50		0.48			38.13	99.11	$(Fe_{0.95}Ni_{0.01})_{0.96}S_{1.04}$

(*Continued*)

https://doi.org/10.1180/mgm.2024.20 Published online by Cambridge University Press

Table 1. (*Continued.*)

No.	Sample, depth	Fe	Co	Ni	Cu	Ag	S	Sum	Formula
68	PT-30_1566	60.75		0.56			38.75	100.06	$(Fe_{0.94}Ni_{0.01})_{0.95}S_{1.05}$
69	PT-30_1566	60.36		0.57			38.71	99.64	$(Fe_{0.94}Ni_{0.01})_{0.95}S_{1.05}$
70	PT-30_1566	60.51		0.60			37.59	98.70	$(Fe_{0.96}Ni_{0.01})_{0.97}S_{1.03}$
71	PT-30_1566	33.13	1.42	31.48			33.59	99.62	$(Fe_{4.58}Ni_{4.14}Co_{0.19})_{8.91}S_{8.09}$
72	PT-30_1566	32.32	1.54	31.82			32.86	98.54	$(Fe_{4.53}Ni_{4.24}Co_{0.20})_{8.97}S_{8.02}$
73	PT-30_1566	31.40	1.65	33.63			33.08	99.76	$(Ni_{4.44}Fe_{4.35}Co_{0.22})_{9.01}S_{7.99}$
74	PT-30_1566	30.68	1.78	33.69			33.20	99.35	$(Ni_{4.46}Fe_{4.27}Co_{0.23})_{8.96}S_{8.04}$
75	PT-30_1566	30.81	1.66	34.25			33.09	99.81	$(Ni_{4.52}Fe_{4.27}Co_{0.22})_{9.01}S_{7.99}$
76	PT-30_1566	29.87			33.14		34.92	97.93	$Cu_{0.97}Fe_{1.00}S_{2.03}$
77	PT-30_1566	38.45			25.44		35.16	99.05	$Fe_{1.89}Cu_{1.10}S_{3.01}$

The table presents the sample compositions of sulfides and is constructed on the principle of changing compositions with depth from the upper parts of the picrite layers to the lower ones for each borehole.
Minerals: 1–14, 49–52, 67–70 – pyrrhotite (Fe,Ni,Co)S; 15–24, 29–39, 53–61, 71–75 – pentlandite $(Fe,Ni)_9S_8$; 25–28 – sugakiite $Cu(Fe,Ni)_8S_8$; 40–46, 62–65, 76 – chalcopyrite $CuFeS_2$; 47–48, 65–66, 77 – cubanite Fe_2CuS_3; * Sample PT-107–1698* – compositions shown in Fig. 7.

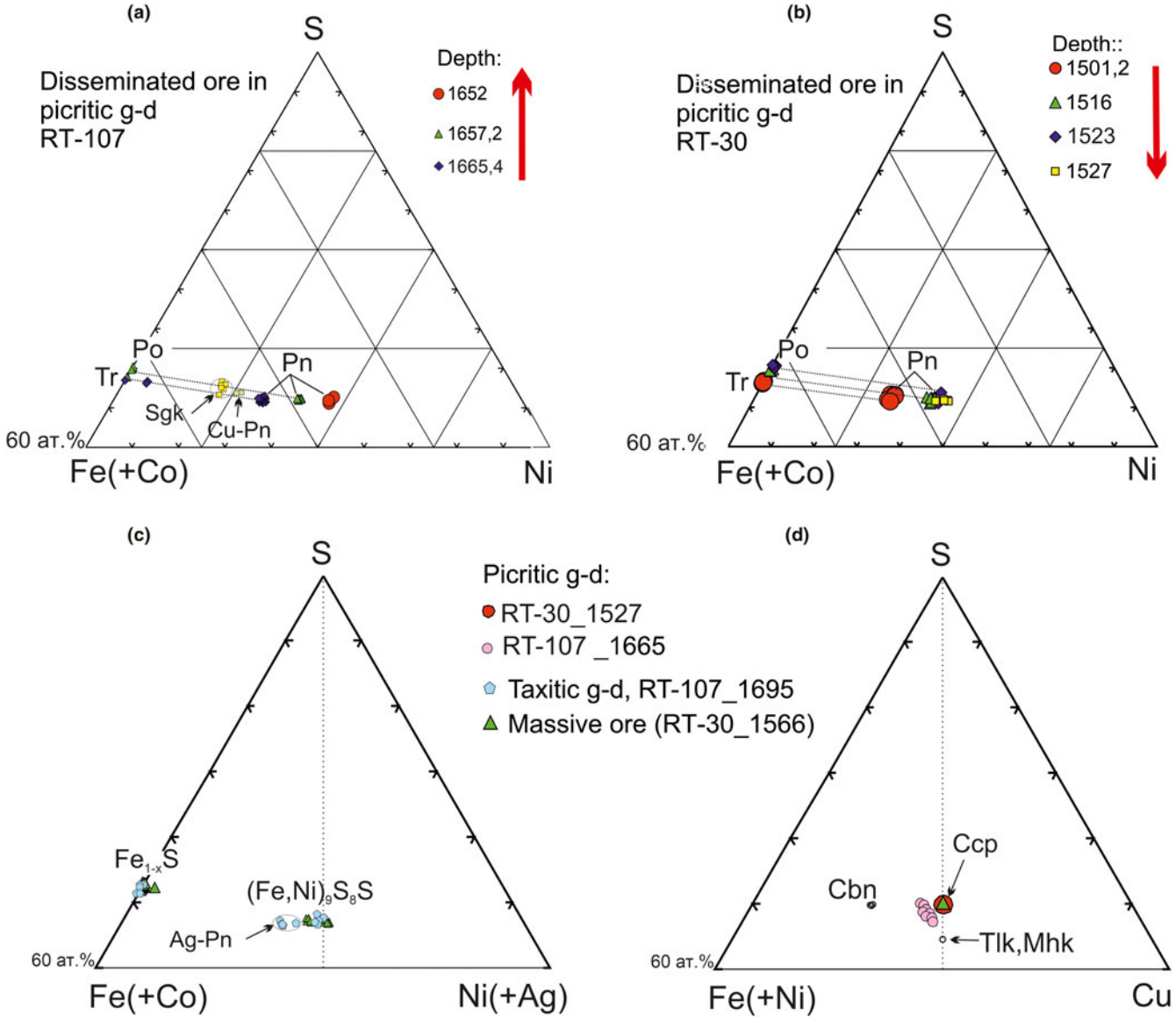

Figure 7. Compositions of sulfides: (a–c) in the Fe(+Co)–S–Ni(+Ag) system; (d) in the Fe(+Ni)–S–Cu system in various types of ores. Details: (a,b) Po and Pn paragenetic associations connected by connodes; (c,d) comparisons of sulfides in picritic, taxitic gabbro-dolerites and massive ores. Po – pyrrhotite, Ccp – chalcopyrite, Pn – pentlandite, Cbn – cubanite, Sgk – sugakiite, Ag-Pn – argentopentlandite, Tlk, Mhk - talnakhite and mooihoekite. The red trend indicates the direction of sulfur fugacity increase.

https://doi.org/10.1180/mgm.2024.20 Published online by Cambridge University Press

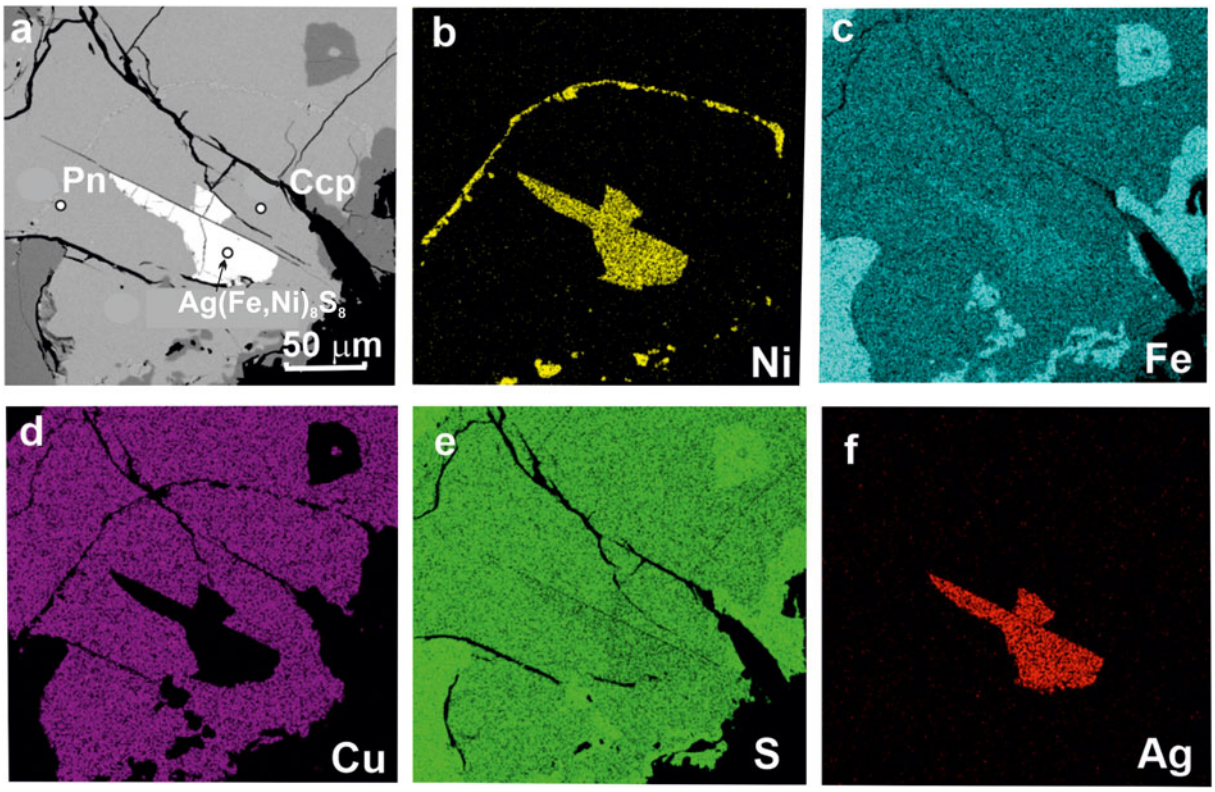

Figure 8. Sulfide microparagenesis in taxitic gabbro-dolerite (RT-107_1695). (a) BSE image of argentopentlandite $Ag(Ni,Fe)_8S_8$ and Ag-free pentlandite (Pn), included in chalcopyrite Ccp and (b–f) X-ray maps of the same area showing individual element distributions.

common mineral of this association. A characteristic feature of this PGM is Au impurity (up to 5.77 wt.%) in atokite and rustenburgite (Table 2). Native silver, Ag–Au–Cu alloys, and auricupride Cu_3Au are common (Table 3, Fig. 12). In the taxitic gabbro-dolerite (in studied samples), only As-bearing paolovite was found up to 0.36 apfu As (Table 2).

Precious metal (PGE and Au) minerals from massive pyrrhotite ores are characterised by platinum specialisation, i.e. all PGMs found are platinum minerals, even though Pd prevails over Pt in all ore samples. They form small (1–3 μm) inclusions in pyrrhotite, less commonly in chalcopyrite. These are represented by Pt–Fe alloys, a S-rich variety of sperrylite PtAsS, sperrylite $PtAs_2$ and cooperite PtS (Fig. 13). The small size of these grains does not always allow determination of the quantitative composition and are hence only identified qualitatively. Only the Au–Ag alloys and cooperite reach sizes of 15–25 μm (Fig. 13a,g). The Au–Ag alloys of this association are of higher grade gold compared to those from the picritic rocks: $Au_{0.64}Ag_{0.36}$ (Table 3, Fig. 12). The concentrations of both Pd and Ni do not exceed 1 wt.% in cooperite (Table 2). A rare associated mineral is bismuth oxychloride with the formula $BiOCl_2$, close to bismoclite (BiOCl) and acanthite Ag_2S, which occur as inclusions up to 10 μm in size in pyrrhotite in massive ores (Fig. 13h,i).

Discussion

Mineralogical features and zoning in picritic gabbro-dolerite of the C-3 and C-4 orebodies

The mineralogy of various types of ores of the Norilsk deposits has been investigated and discussed for many years (for example, Genkin *et al.*, 1969, 1981; Distler *et al.*, 1975, 1999; Genkin and Evstigneeva, 1986; Begizov *et al.*, 1974; Razin *et al.*, 1976; Evstigneeva and Genkin, 1983; Barkov *et al.*, 2000; Kozyrev *et al.*, 2002; Komarova *et al.*, 2002; Spiridonov *et al.*, 2003, 2004, 2015; Likhachev, 2004; Sluzhenikin, 2010, 2011; Sluzhenikin and Mokhov, 2014; Tolstykh *et al.*, 2020a, 2020b, 2021). Our conclusion here is based on mineralogical data which allow us to evaluate the physicochemical conditions of ore crystallisation, in particular, the fugacity of sulfur in the ore-forming system.

The southern and northern orebodies differ in their mineralogical composition. The southern C-4 orebody is characterised by a high-sulfur association and zoning, expressed by pyrrhotite–chalcopyrite fractionation (Distler *et al.*, 1975), and the northern C-3 orebody contains minerals typical of a low-sulfur association (troilite, talnakhite, sugakiite) which is a characteristic of disseminated ores in the picritic gabbro-dolerite only (Distler *et al.*, 1999; Tolstykh *et al.*, 2017).

In addition, these orebodies show multidirectional zoning of pentlandite compositions (Fig. 7), which varies regularly along the sections of the intrusive rocks. The Fe/Ni ratio of pentlandite reflects the activity of sulfur ($\log f_{S_2}$) during its formation, and the Ni content in pentlandite has direct proportional dependence on $\log f_{S_2}$ (Kaneda *et al.*, 1986; Kolonin *et al.*, 2000; Kosyakov *et al.*, 2003). This dependence is based on experimental data and calculation of $k = \mathrm{Ni}/(\mathrm{Ni} + \mathrm{Fe})$ in pentlandite (Fig. 14). The value 'k' varies from 0.38 (in both boreholes, i.e. RT-30 and RT-107), which corresponds to the lowest values of $\log f_{S_2}$ (−13) in the pentlandite stability field, to 0.52 ($\log f_{S_2} = -10.5$) in RT-30 and up to 0.54 ($\log f_{S_2} = -10$) in RT-107. These evolutionary changes are multidirectional in sections of picritic rocks from the different

https://doi.org/10.1180/mgm.2024.20 Published online by Cambridge University Press

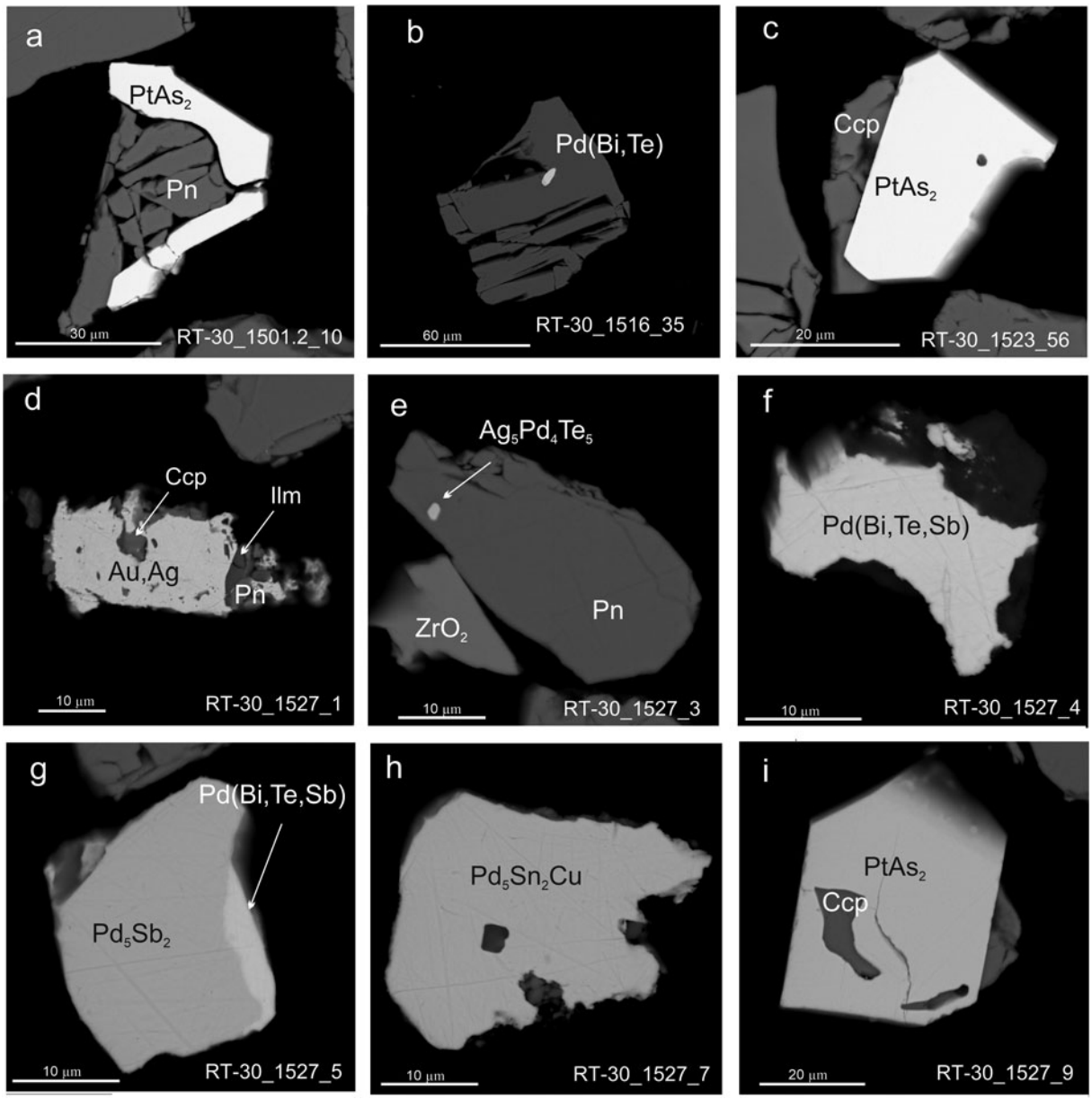

Figure 9. Scanning electron microscope images of PGM and Ag–Au alloys from disseminated ores of picritic gabbro-dolerite of the southern orebody (RT-30): sperrylite $PtAs_2$ intergrown with pentlandite (a) and chalcopyrite (c, i); sobolevskite Pd(Bi,Te,Sb) and Pd(Bi,Te) (b,f); sopcheite $Ag_5Pd_4Te_5$ included in pentlandite (e); stibiopalladinite Pd_5Sb_2 intergrown with sobolevskite (g); grain of stannopalladinite Pd_5Sn_2Cu (h).

orebodies of the Oktyabr'sky deposit (Fig. 15). Our data shows that the Ni/(Ni + Fe) ratio of pentlandite and S in pyrrhotite increases with depth in the disseminated ore of the southern body (borehole RT-30 from 1501.2 m to 1527 m); consequently, the fugacity of sulfur increases and the evolution of the sulfide melt occurs in the same direction. In contrast, the picritic gabbro-dolerite from borehole RT-107 (northern C-4 orebody) shows an opposite zoning trend with Fe-enriched pentlandite and troilite characteristic of the deeper 1665.4 m horizon, and with the Ni/(Ni + Fe) ratios of pentlandite increasing upwards in the section (Fig. 7a,b). Consequently, the evolution of the sulfide melt increases from the bottom to the top along the picritic rock of the C-3 orebody (i.e. reverse zoning).

Mineralogical zoning in the picritic gabbro-dolerite has been described previously and shown to be from a low-sulfur association with troilite, talnakhite, cubanite and Fe-rich pentlandite in the upper most magnesian part to a high-sulfur association at its base (Distler *et al.*, 1999). The same direction of evolution of the sulfide parageneses from top to bottom was also observed in the picritic gabbro-dolerite of the Norilsk 1 intrusion (Tolstykh *et al.*, 2020b, 2021). Sluzhenikin (2010) showed that in picritic rocks zoning is directed in both directions from the central part towards the top and bottom, in addition to relative increase in the sulfur content of parageneses.

The zoning of the disseminated ores in different boreholes as identified in this work coincides with the evolution vectors shown for the massive sulfide lenses with similar composition (Torgashin, 1994; Fig. 3). These massive lenses also have opposite vertical mineralogical and geochemical zoning. The lenses of cubanite–chalcopyrite ore are characterised by an

https://doi.org/10.1180/mgm.2024.20 Published online by Cambridge University Press

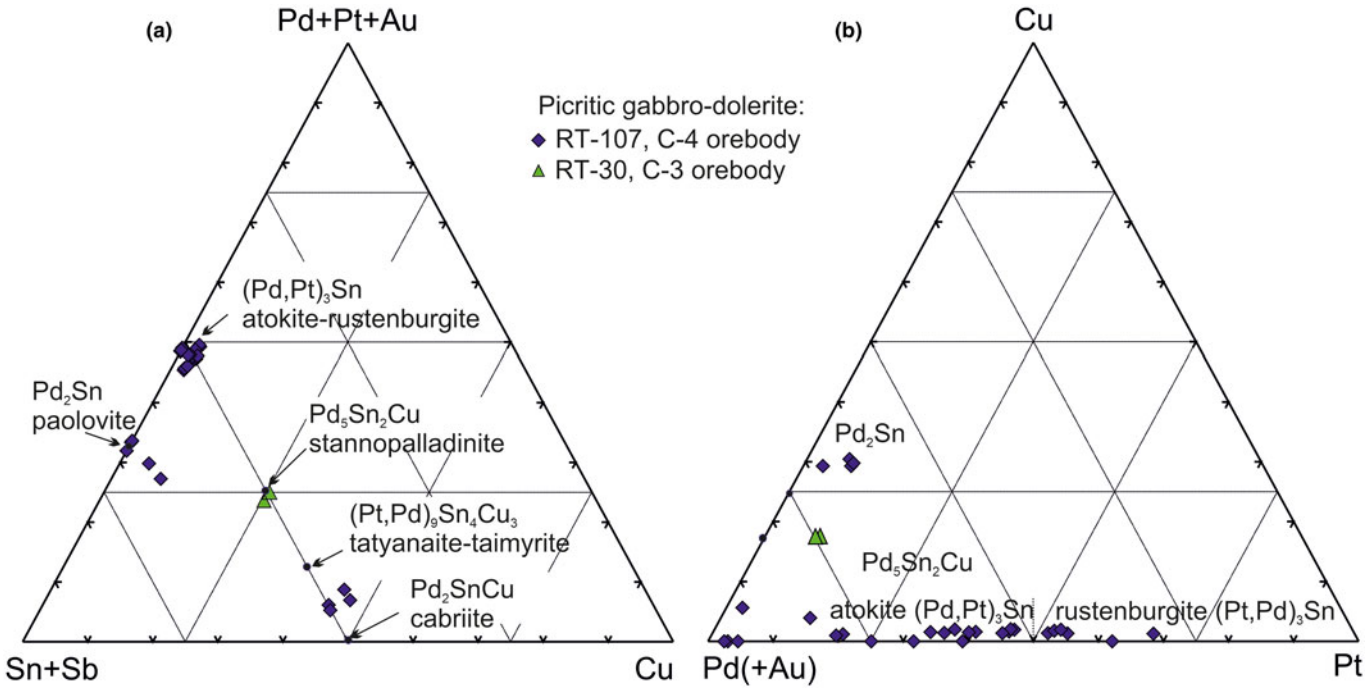

Figure 10. Compositions of PGE minerals in the Sn–(Pd + Pt)–Cu (a) and Pd(+Au)–Cu–Pt (b) systems.

Table 2. Compositions of PGM (wt.%).

No.	Sample	Ni	Pt	Pd	Cu	Au	Sn	Sb	Te	As	Bi	S	Total	Formula
Disseminated ores in picritic gabbrodolerite														
1	PT-30_1501.2		55.81							42.75			98.56	$Pt_{1.00}As_{2.00}$
2	PT-30_1501.2		55.65							42.36			98.01	$Pt_{0.98}As_{2.02}$
3	PT-30_1527		54.72							43.37			98.09	$Pt_{0.98}As_{2.02}$
4	PT-107_1657.2		55.61							41.56			97.17	$Pt_{1.02}As_{1.98}$
5	PT-107_1665.4		56.33							41.78			98.11	$Pt_{1.02}As_{1.98}$
6	PT-107_1665.4		55.64							41.94			97.58	$Pt_{1.01}As_{1.99}$
7	PT-30_1516			36.99					19.43		42.11		98.53	$Pd_{0.99}(Bi_{0.57}Te_{0.44})_{1.01}$
8	PT-30_1516			36.73					19.14		42.03		97.90	$Pd_{0.99}(Bi_{0.58}Te_{0.43})_{1.01}$
9	PT-30_1527			36.25				2.08	11.88		48.15		98.36	$Pd_{1.00}(Bi_{0.68}Te_{0.27}Sb_{0.05})_{1.00}$
10	PT-30_1527			36.37				2.25	11.97		46.76		97.35	$Pd_{1.01}(Bi_{0.66}Te_{0.28}Sb_{0.05})_{0.99}$
11	PT-30_1527			36.57				1.71	21.64		38.29		98.21	$Pd_{0.97}(Bi_{0.52}Te_{0.48}Sb_{0.04})_{1.04}$
12	PT-30_1527			36.87				3.99	17.26		39.95		98.07	$Pd_{0.98}(Bi_{0.54}Te_{0.38}Sb_{0.09})_{1.01}$
13	PT-30_1527			66.70				31.12					97.82	$Pd_{4.97}Sb_{2.03}$
14	PT-107_1652		60.00				37.65						97.65	$Pt_{0.98}Sn_{1.02}$
15	PT-107_1652		60.01				37.39						97.40	$Pt_{0.99}Sn_{1.01}$
16	PT-107_1665.4		5.25	59.46			34.53						99.24	$(Pd_{1.91}Pt_{0.09})_{2.00}Sn_{1.00}$
17	PT-107_1665.4		3.49	61.00			35.06						99.55	$(Pd_{1.94}Pt_{0.06})_{2.00}Sn_{1.00}$
18	PT-107_1665.4		2.86	61.44			32.92	3.41					100.63	$(Pd_{1.93}Pt_{0.05})_{1.98}(Sn_{0.93}Sb_{0.09})_{1.02}$
19	PT-30–1527		12.01	53.64	7.52		25.64	2.01					100.82	$(Pd_{4.40}Pt_{0.54})_{4.94}(Sn_{1.89}Sb_{0.14})_{2.03}Cu_{1.03}$
20	PT-30–1527		10.98	53.58	7.42		25.90						97.88	$(Pd_{4.50}Pt_{0.50})_{5.00}Sn_{1.95}Cu_{1.04}$
21	PT-107_1652		57.89	16.61		4.9	19.57						98.97	$(Pt_{1.85}Pd_{0.97}Au_{0.15})_{2.97}Sn_{1.03}$
22	PT-107_1665.4		21.85	46.43	0.36	5.77	23.47						97.88	$(Pd_{2.23}Pt_{0.57}Au_{0.15}Cu_{0.03})_{2.98}Sn_{1.01}$
23	PT-107_1665.4		35.73	36.57	0.53	2.51	21.43	1.24					98.01	$(Pd_{1.86}Pt_{0.99}Au_{0.07}Cu_{0.05})_{2.97}(Sn_{0.98}Sb_{0.06})_{1.04}$
24	PT-107_1665.4		39.30	34.09	0.69	2.55	21.15						97.78	$(Pd_{1.77}Pt_{1.11}Au_{0.07}Cu_{0.06})_{3.01}Sn_{0.98}$
25	PT-107_1665.4		45.66	29.12	0.46	2.05	20.81	1.27					99.37	$(Pd_{1.54}Pt_{1.32}Au_{0.06}Cu_{0.04})_{2.96}(Sn_{0.99}Sb_{0.06})_{1.05}$
26	PT-107_1665.4		63.27	15.72	0.39		18.87						98.25	$(Pt_{2.04}Pd_{0.93}Cu_{0.04})_{3.01}Sn_{1.00}$
27	PT-107_1665.4		10.11	46.39	13.2		27.54						97.19	$(Pd_{1.88}Cu_{0.89}Pt_{0.22})_{2.99}Sn_{1.00}$
28	PT-107_1665.4		4.18	51.5	13.3		28.2						97.18	$(Pd_{2.03}Cu_{0.88}Pt_{0.09})_{3.00}Sn_{1.00}$
Disseminated ores in taxitic gabbro-dolerite														
29	PT-107_1695			65.68			23.58			8.26			97.52	$Pd_{2.00}(Sn_{0.64}As_{0.36})_{1.00})$
30	PT-107_1695			62.09			34.77						96.86	$Pd_{2.00}Sn_{1.00}$
Massive ore														
31	PT-30_1566	0.84	83.04	1.06								14.69	99.63	$(Pt_{0.94}Ni_{0.03}Pd_{0.02})_{0.99}S_{1.01}$
32	PT-30_1566	0.71	82.94	0.77								14.57	98.99	$(Pt_{0.95}Ni_{0.03}Pd_{0.02})_{1.00}S_{1.00}$
33	PT-30_1566	0.79	83.05	0.70								14.78	99.32	$(Pt_{0.94}Ni_{0.03}Pd_{0.01})_{0.98}S_{1.02}$
34	PT-30_1566	0.90	81.03	0.90								14.65	97.48	$(Pt_{0.93}Ni_{0.03}Pd_{0.02})_{0.98}S_{1.02}$
35	PT-30_1566	0.52	84.60									15.02	100.14	$(Pt_{0.95}Ni_{0.02})_{0.97}S_{1.03}$

* The total of the mineral analysis after subtracting the composition of the sulfide matrix; Minerals: 1–6 – sperrylite $PtAs_2$; 7–12 – sobolevskite Pd(Bi,Te,Sb); 13 – stibiopalladinite Pd_5Sb_2; 14, 15 – niggliite PtSn; 16–18, 29–30 – paolovite $Pd_2(Sn,As,Sb)$; 19–20 – stannopalladinite Pd_5Sn_2Cu; 21–26 - rustenburgite-atokite solid solutions $(Pd,Pt,Cu)_3Sn$; 27–28 – taimyrite–cabriite solid solution $(Pd,Pt,Cu)_3Sn$; 31–35 – cooperite PtS.

https://doi.org/10.1180/mgm.2024.20 Published online by Cambridge University Press

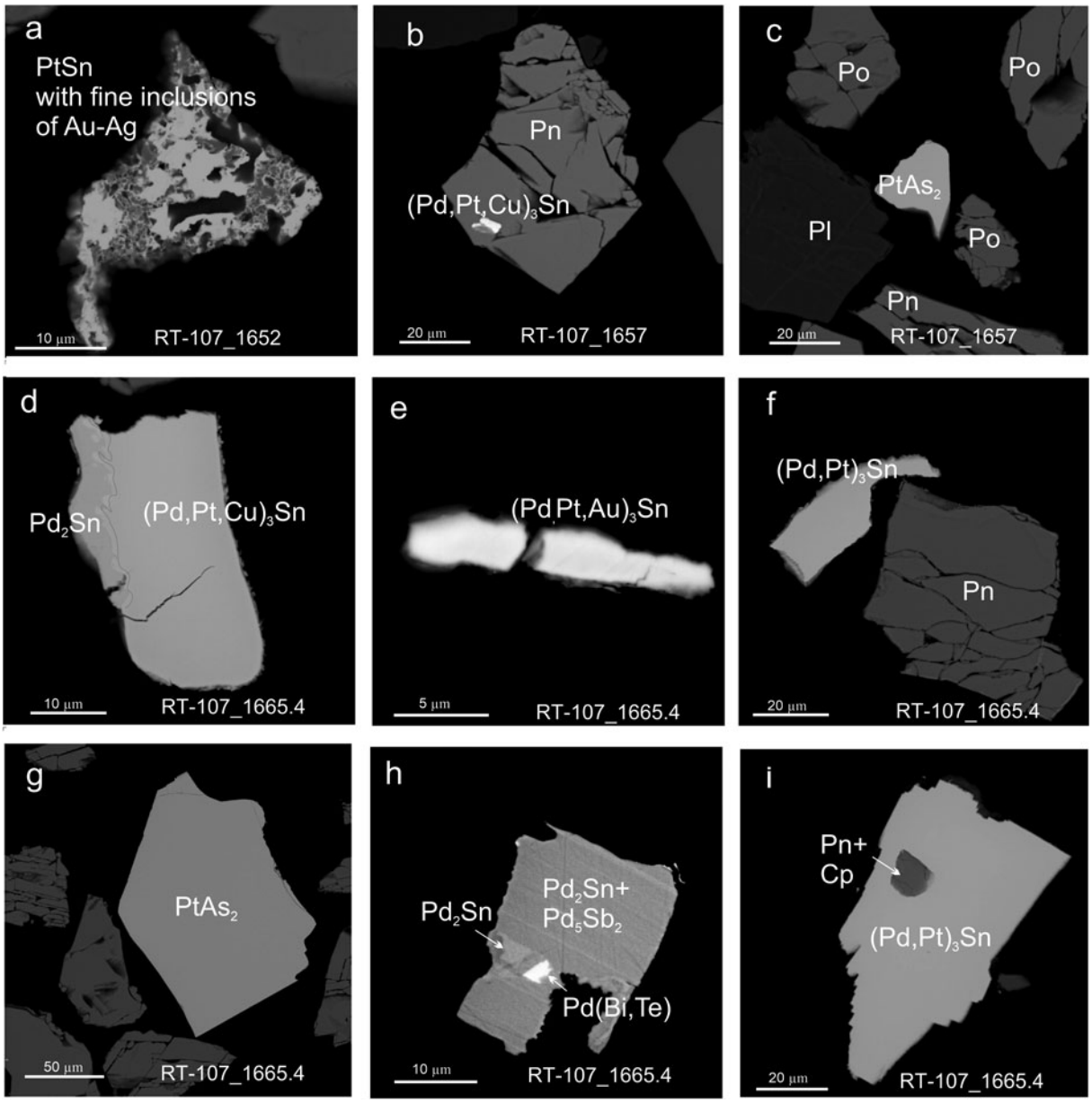

Figure 11. SEM images. PGM from disseminated ore of picritic gabbro-dolerite of the northern orebody (borehole RT-107: (a) niggliite PtSn; (b,d,f,i) – rustenburgite $(Pd,Pt,Cu)_3Sn$; (c,g) – sperrylite $PtAs_2$; (e) stannopalladinite Pd_5Sn_2Cu; (h) inclusions of sobolevskite Pd(Bi,Te) and paolovite Pd_2Sn in the exsolution texture of paolovite and stibiopalladinite Pd_5Sb_2.

Table 3. Compositions of Au–Ag alloys from the Oktyabr'sky deposit.

No.	Sample_depth	Au Wt.%	Ag	Cu	Total	Au At.%	Ag	Cu	Total
Disseminated ores in picritic gabbrodolerites (Orebody C-4)									
3	PT-107_1665.4		98.48		98.48		100.0		100.0
4	PT-107_1665.4		99.82		99.82		100.0		100.0
5	PT-107_1665.4	49.91		47.89	97.8	25.16	0.00	74.84	100.0
6	PT-107_1665.4	49.18		47.15	96.33	25.18	0.00	74.82	100.0
7	PT-107_1665.4	39.98	43.93	14.21	98.12	24.34	48.84	26.82	100.0
8	PT-107_1665.4	39.26	59.92	2.13	101.31	25.28	70.46	4.25	100.0
9	PT-107_1665.4	40.03	58.82	2.96	101.81	25.56	68.58	5.86	100.0
Massive ore (Orebody C-3)									
1	PT-30_1566	71.25	23.17		94.42	62.74	37.26		100.0
2	PT-30_1566	70.5	22.36		92.86	63.33	36.67		100.0

https://doi.org/10.1180/mgm.2024.20 Published online by Cambridge University Press

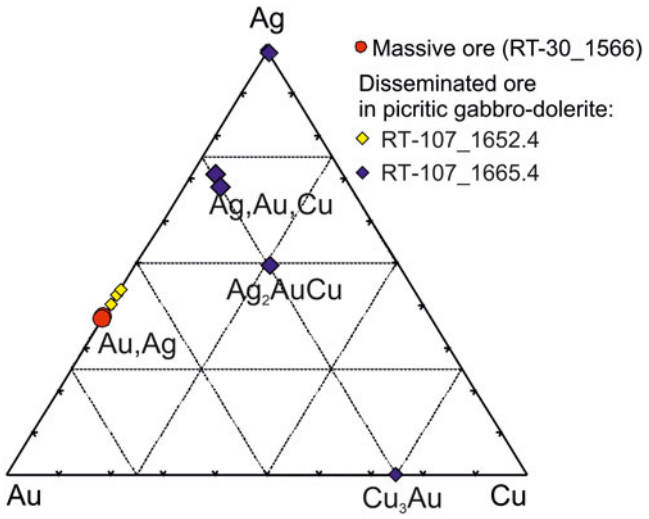

Figure 12. Compositions of Au–Ag–Cu alloys in various types of ores from the C-3 and C-4 orebodies.

increase in incompatible elements from the bottom to the top along the section similar to that of the southern C-3 orebody. In contrast, the ores in the pyrrhotite domain evolve from the top to the bottom, along the vertical section as in the northern C-4 orebody.

PGE minerals from disseminated ore in the picritic gabbro-dolerite

The compositions of disseminated ores from different rocks and the paragenesis of sulfide minerals in the picritic and taxitic gabbro-dolerites have been established for the Norilsk 1, Oktyabr'sky and Talnakh deposits (Genkin *et al.*, 1977; Naldrett, 2004; Distler *et al.*, 1979, 1999; Spiridonov, 2010; Tolstykh *et al.*, 2020b). Note that sometimes disseminated ores from the picritic and taxitic gabbro-dolerites are combined during research and considered together as one 'Main Ore Horizon' (Komarova *et al.*, 2002).

Using the example of the Norilsk 1 intrusion, we showed (Tolstykh *et al.*, 2021) that the picritic and taxitic gabbro-dolerites differ in mineral associations, although they are characterised by the same type of zoning in relation to PGMs. Namely, from Pd–Sn–Cu minerals common in the upper parts of both layers to the minerals of the Pd–Bi–Sb and Pd–Bi systems characteristic of the base of each layer, in accordance with the regressive temperature gradient and the direction of PGE fractionation in the sulfide melt. Such a distribution of PGMs characterises reverse zoning.

The PGM associations in the C-3 and C-4 orebodies are also unevenly distributed. At the base of the picritic gabbro-dolerite of the C-4 orebody, the leading minerals are high-temperature PGMs of the Pd–PT–Cu–Sn system: atokite–rustenburgite (Pd, Pt)$_3$Sn; cabriite Pd_2CuSn; and paolovite Pd_2Sn, which correspond to direct zoning. Whereas, at the base of picritic gabbro-dolerite of the C-3 orebody, low-temperature PGMs of the Pd–Bi–Te–Sb system, e.g. sobolevskite Pd(Bi,Te), are widespread in accordance with the reverse zoning of the development of the ore-forming system (Fig. 15).

The modes of occurrences of Au and Ag also differ in that only silver telluride (sopcheite) was found in the southern C-3 orebody, whereas native alloys (Ag, Au and Cu) are typical for the northern C-4 orebody and are enriched in Au at a higher level. Thus, the PGE-bearing ore-forming systems of picritic gabbro-dolerite differ in different orebodies in the Oktyabr'sky deposit penetrated by RT-30 and RT-107 boreholes (Fig. 16a,b).

Mineralogical similarities and differences between disseminated and massive ores in the southern orebodies.

Massive ore in the exocontact of the intrusion and disseminated ore in the picritic gabbro-dolerite of a section along the RT-30 borehole of the southern C-3 orebody have both differences and similarities. The main difference is in the features of PGM mineralisation. Whereas the Pd–Bi–Sb–Te minerals are common in the disseminated ores, the massive ores contain only Pt minerals, among which cooperite PtS is more common (Fig. 16c). This characteristic of massive ores makes them comparable with other pyrrhotite ores of the Norilsk region (Kozyrev *et al.*, 2002), though not with disseminated ores in the picritic rocks.

Nevertheless, the similarity lies in the unidirectional mineralogical and geochemical zoning from the top to the bottom along the cross-section, due to the evolution of the sulfide melt (Fig. 15). It is assumed that zoning in the pyrrhotite ores of the C-3 body is analogous to zoning in the pyrrhotite lens of the Main Ore Body of the Oktyabr'sky deposit, where the concentration of Cu and incoherent elements increases down the section (Torgashin, 1994, Fig. 3).

This unidirectional evolution seems logical if one follows the hypothesis that the massive ores are the result of the deposition of sulfide droplets from disseminated horizons and their infiltration into the underlying rocks through the taxitic and contact gabbro-dolerite. Barren hornfelses at the contact of disseminated and massive ores, sharp changes in sulfide parageneses between picritic and taxitic gabbro-dolerites (Tolstykh *et al.*, 2020b), as well as a significant difference in PGM associations between disseminated and underlying massive ores do not comform to this hypothesis. If we consider disseminated and massive ores as different episodes of long-term magmatic activity (Zientek and Likhachev, 1992), then unidirectional trends (evolutionary zoning) of massive and disseminated ores can be caused by the action of similar mechanisms of intrusion of silicate magma (with droplets of sulfides) and sulfide melts.

Features of rare sulfides from various types of ores

Argentopentlandite $Ag(Ni,Fe)_8S_8$ occurs in taxitic gabbro-dolerite (RT-107_1695) of the C-4 orebody. This mineral was also found in various ores of the Norilsk deposits, and it can be associated concurrently with ordinary pentlandite and Ag-bearing pentlandite (Sluzhenikhin and Mokhov, 2014), as found in this study. Silver can only occupy an octahedral site in argentopentlandite, thus its amount should not exceed 1 apfu of Ag in the structure of the mineral (Hall and Stewart, 1973; Rudashevskii *et al.*, 1977), which corresponds to the formula $Ag(Fe,Ni)_8S_8$ or, more precisely, $AgFe_6^{2+}Ni_2S_8$, in which Fe predominates three times over Ni, which is also characteristic of the argentopentlandite investigated (Table 1). Argentopentlandite might be a product of exsolution from an Ag-bearing intermediate solid solution during the cooling of the ore-forming system according to one of the models described in Melfos *et al.* (2001). Taking into account its morphological character of segregations as relatively large grains (60–70 μm) in the chalcopyrite matrix, located in the halo of

https://doi.org/10.1180/mgm.2024.20 Published online by Cambridge University Press

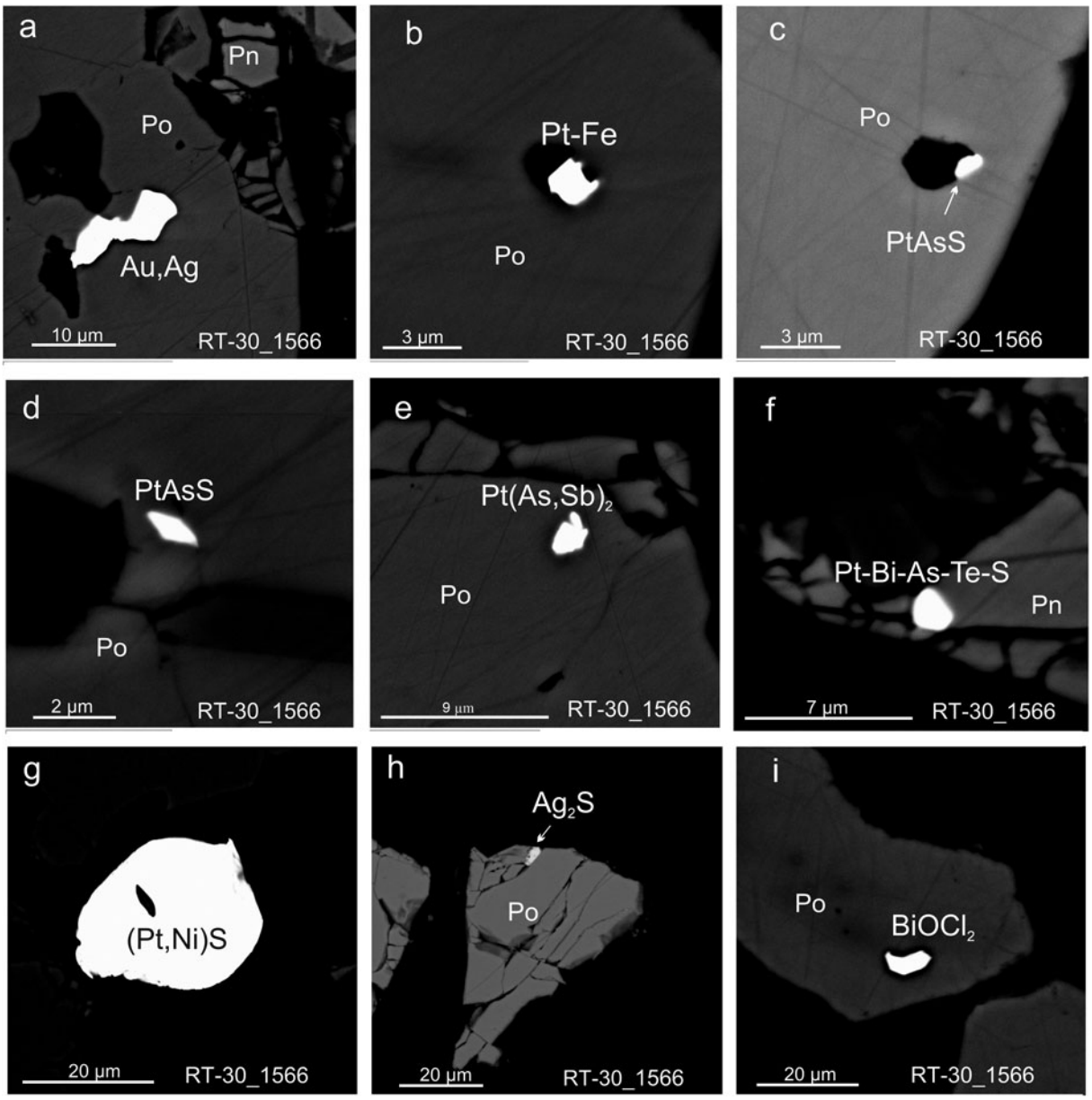

Figure 13. SEM images of PGM, gold and associated minerals from massive ore of the C-3 orebody (RT-30_1566 m). Inclusions of (a) Au–Ag alloy; (b) isoferroplatinum Pt_3Fe, (c,d) S-rich variety of sperrylite PtAsS, (e) Sb-sperrylite, (f) Pt–Bi–As–Te–S phase, (g) cooperite grain, (h) acanthite (Ag_2S), (i) bismoclite in pyrrhotite.

small Ag-free pentlandite grains (Fig. 8), it can be assumed that argentopentlandite is an early mineral and crystallises under the less sulfuric conditions of the ore-forming system of the taxitic gabbro-dolerite. With a decrease in temperature and an increase in sulfur fugacity, small grains of more nickel-rich pentlandite crystallised from residual melts in the intergranular space surrounding chalcopyrite grains, the composition of which corresponds to the $\log f_{S_2} = -10$ to -10.5.

Sugakiite as large (~80 μm) granular grains is common in the picritic gabbro-dolerite of the C-4 orebody. It is assumed that sugakiite crystallised due to the peritectic reaction of Mss with melt, similar to early pentlandite Pn_1 (Distler *et al.*, 1996), though only under conditions of low sulfur activity, which is noted at the base of the picritic rocks in the RT-107 borehole. Sugakiite is not an exsolution product, as this mineral contains up to 0.9 apfu Cu that is in excess in the residual melt, but does not fractionate in Mss. The ratio Ni/(Ni + Fe) of sugakiite is the lowest (0.26–0.27) compared to pentlandite of all horizons of the picritic rock in borehole RT-107. Compositions of sugakiite are mostly moved to the ferruginous area of the diagram (Fig. 7a). This mineral intergrows with troilite, so it can be assumed that it crystallised under conditions of the lowest sulfur fugacity that were achieved at the base of the picritic layer of the C-4 orebody. Sugakiite is a very rare mineral of low sulfur association discovered in sulfide aggregates in a peridotite of the Horoman massif, Hokkaido, Japan (Kitakaze, 2008). Sugakiite has also been noted in picritic gabbro-dolerite of the C-6 orebody located in the northeastern part of the Oktyabr'sky deposit, in which the massive ores are also essentially pyrrhotite (Ketrov *et al.*, 2022).

Origin of different types of sulfide ores

There is a hypothesis that the Kharaelakh intrusion is a single horizontal channel of magma supplied to the surface (chonolith),

https://doi.org/10.1180/mgm.2024.20 Published online by Cambridge University Press

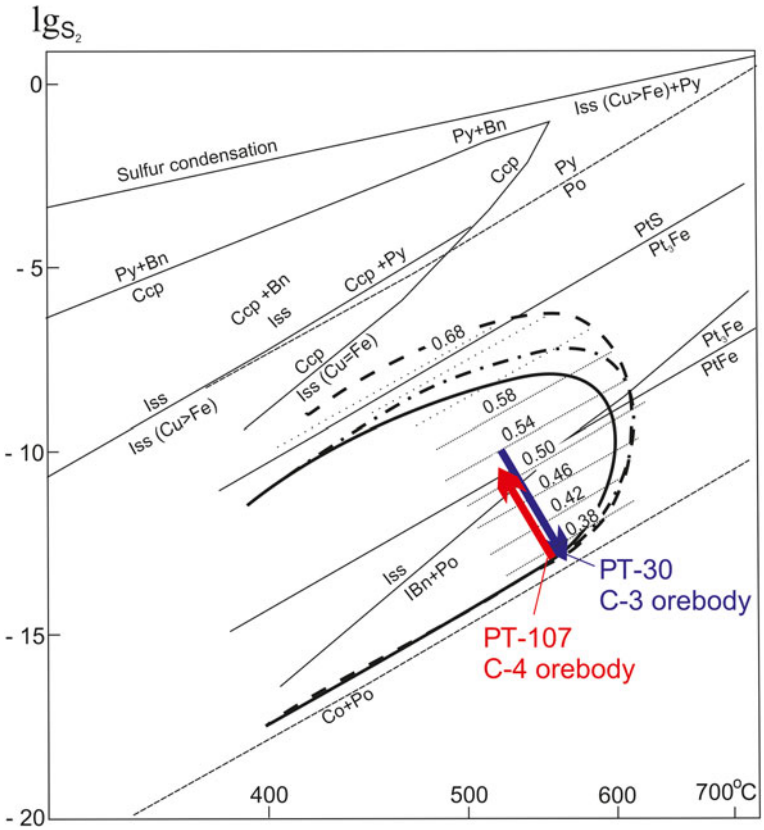

Figure 14. Physical and chemical conditions for the formation of pentlandite and Pt minerals relative to phase equilibria for the Cu – Fe – S and Ni – Fe – S systems (from Kolonin *et al.*, 2000). The solid elliptical curve is the boundary of the field of stability of pentlandite from Vaughan and Craig (1981), the dotted-dashed curve is from Kolonin *et al.* (2000), and the dotted curve from Peregoedova (1999). The dotted lines within the pentlandite field indicate the changing value of $k = Ni/(Ni + Fe)$ with decreasing temperature and increasing sulphur volatility. The vectors indicate the evolution of pentlandite in the picritic gabbro-dolerite from bottom to top along the cut of layers: RT-107 (red) and RT-30 (blue).

in which, upon interaction with the host rocks, a sulfide melt segregated and formed the orebodies (Rad'ko, 1991). Others have suggested two-stage (Zolotukhin *et al.*, 1975), three-stage (Turovtsev, 2002; Malitch *et al.* 2010) or multipulse (Zientek and Likhachev, 1992; Likhachev, 1996) formation of the Kharaelakh intrusion. An extended period of magmatic activity from Middle Palaeozoic to Early Mesozoic consistent with multiple magmatic events during the evolution of the Kharaelakh intrusion has been assumed. The interaction of juvenile and crustal magmatic sources with a mantle origin based on Hf–Nd isotope data has been established (Malich *et al.*, 2010). The multipulse concept is consistent with our mineralogical studies of the central part of the Oktyabr'sky deposit, where the intrusion and crystallisation of differently fractionated melts was occurring in the southern and northern orebodies. Each magma pulse generated its own cooling front on a local scale, forming forward zoning in the northern C-4 orebody, and reverse zoning in the southern C-3 orebody. The high ore/silicate imbalance and complex mineralogical and geochemical zoning confirms a dynamic mode for the origin of ore-bearing intrusions and a pulsed nature of magma intrusion with different evolutionary histories of the sulfide melts in the C-3 and C-4 orebodies.

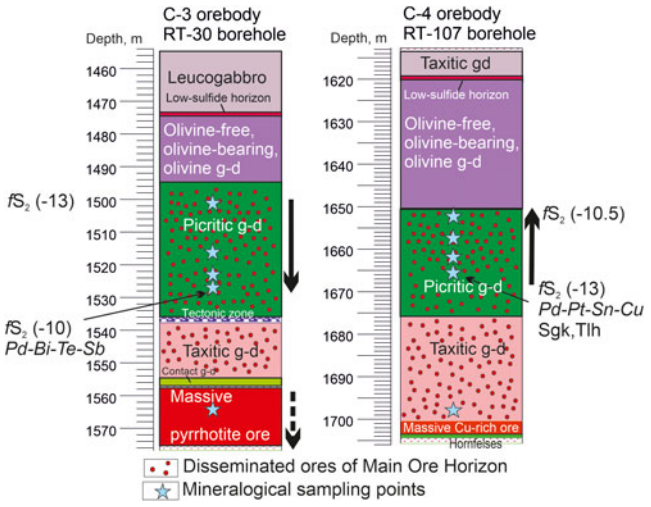

Figure 15. Parameters of sulfur volatility (fS_2) and directions of evolution of the sulfide melt (trends) in the sections of the southern (RT-30) and northern (RT-107) orebodies of the Oktyabr'sky deposit. The distribution of minerals of various systems in the sections is shown by arrows. Sgk – sugakiite and Tlh – talnakhite.

It is assumed that the disseminated ores were formed as a result of the intrusion of silicate magma containing sulfide liquid, the segregation of which occurred throughout the entire period of existence of the magmatic melt (Zientek and Likhachev, 1992; Likhachev, 1973, 2006). Volatiles in the magma played a significant role in the carrying capacity of rising magma in transporting sulfide droplets. To explain the formation of globular disseminated ores in picritic gabbro-dolerites, models of the so-called 'segregation vesicles' attached to sulfide liquid droplets have been proposed. Segregation vesicle disruption is considered to have occurred *in situ* at low pressures, resulting in the release of sulfide liquids that could accumulate in traps. However, 'bubble-rafting' according to Yao *et al.* (2019) and Barnes *et al.* (2019) was not the predominant mechanism of ore formation. It has been noted (Yao *et al.*, 2019) that the mechanisms of evaporite assimilation *in situ* and high *R*-factor do not need to be involved for the formation of disseminated ores.

The formation of massive ores, according to Likhachev (2006) is the result of sulfide liquid settling in widened sections of

https://doi.org/10.1180/mgm.2024.20 Published online by Cambridge University Press

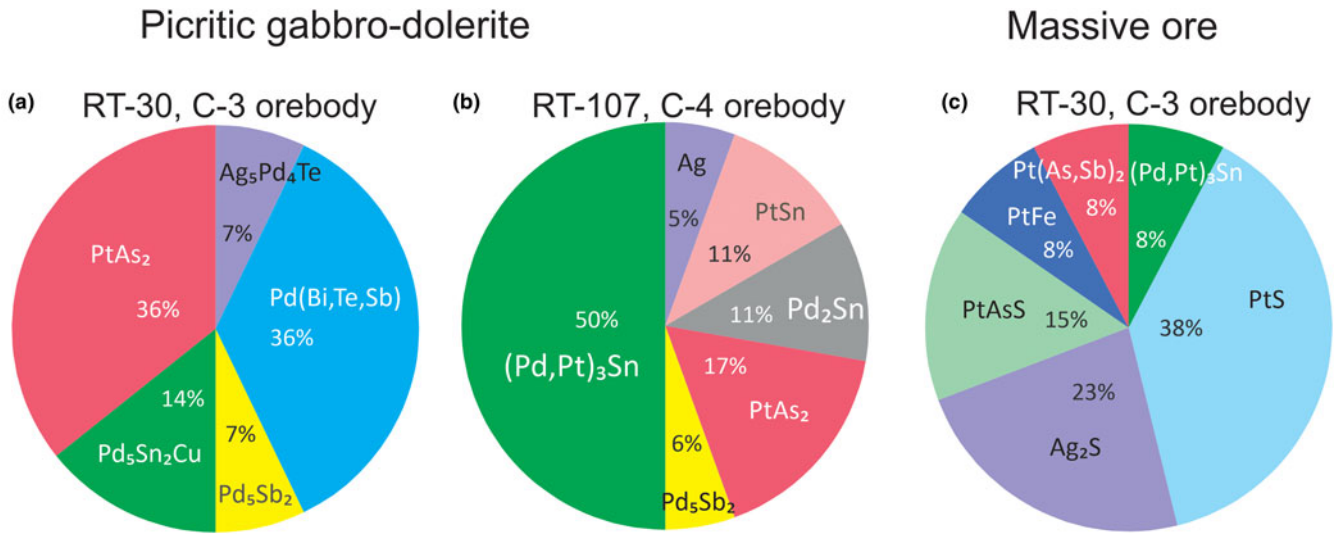

Figure 16. The ratio of platinum-group minerals in disseminated ores from picritic gabbro-dolerite from the southern (RT-30) and northern (RT-107) orebodies of the Oktyabr'sky deposit (a,b) and in massive ores (c).

magma channels, where magma flow slowed. In our case, it is also unlikely that massive ores could be a result of permanent settling of sulfide droplets to the bottom of the formation chamber and the penetration of the accumulated sulfide melt through the layers of taxitic and contact gabrodolerites into the underlying rocks. The arguments are: (1) disseminated ores in picritic gabbro-dolerites and massive ores have completely different sulfide assemblages and PGM compositions; (2) there is a distinct geochemical and mineralogical contrast between picritic and the underlying taxitic ores (Tolstykh *et al.*, 2017, 2020b, 2021), rather than gradual changes in composition, as would occur with sequential droplet deposition; and (3) there is a gap between disseminated and massive ores, containing a layer of barren rocks. There is also a hypothesis that disseminated ore in the gabbro-dolerites are enriched in 'fractional sulfide fluid coming from underlying massive sulfide ores' (Naldrett, 2004). This seems unlikely as there is a layer of barren hornfelses between the massive ore and taxitic gabbro-dolerite (Fig. 5).

It is obvious that the formation of disseminated and massive ores are fragments of two different intrusion processes from one intermediate chamber as the geochemical features, namely the PGE distribution patterns, are the same for all types of ores, but with different degrees of element fractionation (Tolstykh *et al.*, 2020b). It can be assumed that the magmatic system first functioned as an open system and filled the pools in a single act in the case of direct zoning in the C-4 orebody or multi-act in the case of reverse zoning in the C-3 orebody. Subsequently, the magmatic system could close, giving preference to crystallisation fractionation at the final stage.

The formation of reverse zoning in the marginal parts of layered intrusions is a controversial issue (Latypov *et al.*, 2007, 2011; Latypov and Egorova, 2012; Egorova and Latypov, 2013; Egorova and Shelepayev, 2020 and references therein). These authors summarised numerous reasons potentially leading to the reverse zoning, suggesting, among other ideas, that top-down crystallisation of ore matter was due to: (1) the floating of early Mss crystals towards the roof; (2) a progressive decrease in the amount of trapped residual liquid; or (3) top-down solidification from a cold roof rock. However, these factors are debatable and in each specific case they might vary in importance.

In our opinion, the most appropriate petrological mechanisms for reverse zoning formation is the filling of the magma chamber with the continuous arrival of increasingly primitive melt, which was fractionated in the supply channel or in the intermediate chamber (Egorova and Latypov, 2013). This mechanism is most consistent with the zoning in the C-3 orebody, and observed in the rocks in the Norilsk 1 intrusion (Tolstykh *et al.*, 2020b).

The process of fractional crystallisation was most probably the leading one, as both types of zoning (direct and reverse) correspond to the evolution of the sulfide melt. In the first case *in situ* (in the chamber of formation), and in the second in an intermediate chamber or supply channel, if we accept the hypothesis of a continuous flow of increasingly primitive melts (Latypov *et al.*, 2007, 2011).

Conclusions

The southern C-3 orebody of massive ores penetrated by borehole RT-30, is composed mainly of pyrrhotite, and is comparable to the pyrrhotite lenses, whereas the northern C-4 orebody, composed of talnakhite–chalcopyrite ores penetrated by the RT-107 borehole, can be compared with the Cu-rich lenses of the Main Ore Body of the Oktyabr'sky deposit.

The southern and northern orebodies differ in their mineral compositions. The former is characterised by a high-sulfur association, and the latter contains minerals with a deficit of sulfur. Multidirectional evolution of the ore-forming systems is observed in the disseminated ores of these deposits. In the northern C-4 orebody direct crystallisation zoning is observed, where the fugacity of sulfur increases from the bottom to the top, whereas in the southern C-3 orebody f_{S_2} decreases in this direction. The zoning coincides with the evolutionary vectors of various 'blocks' of the massive Main Ore Body ores of the Oktyabr'sky deposit. The presence of the rare mineral, sugakiite, in the lower part of the picritic gabbro-dolerite of the northern orebody is confirmed by the extremely low values of sulfur fugacity, which increase upwards in the section.

Platinum-group mineral associations and modes of occurrence of Au and Ag in the northern and southern orebodies also differ and correspond to sulfide zoning. In the lower horizon of picritic

https://doi.org/10.1180/mgm.2024.20 Published online by Cambridge University Press

gabbro-dolerite of the northern C-4 orebody. The leading compounds are high-temperature PGM of Pd–PT–Cu–Sn systems in accordance with direct zoning, whereas in the lower horizon of the southern C-3 orebody the low-temperature PGMs of the Pd–Bi–Te–Sb system are widespread in accordance with the reverse zoning of the evolution of ore-forming systems.

Disseminated and massive ores within a single cross-section of borehole RT-30 of the southern orebody are different in mineral associations in that the former is characterised by minerals of the Pd–Bi–Sb–Te system, whereas the latter is characterised only by Pt-minerals. The similarity of these ores lies in the unidirectional reverse mineralogical and geochemical zoning along the cross-sections in both disseminated and massive ores, which are the result of different magmatic events. However, unidirectional zoning of both types of ores might be due to the action of the same type of mechanism.

All the above data indicate that the formation of the southern C-3 and northern C-4 orebody occurred under different physicochemical conditions as the result of the intrusion of various portions of both ore-silicate magmas, from which disseminated ores were formed, together with sulfide melt, previously separated into copper-rich and iron-rich fractions in the intermediate chamber. Each of the portions entered the formation chambers through different magma channels.

Acknowledgments. We thank analysts M. Khlestov for carrying out analytical procedures and providing quantitative analyses, and N. Belkina and M. Podlipsky for technical assistance in the manuscript preparing. Funding: This research was carried out within the framework of the state assignment of the IGM SB RAS financed by the Ministry of Science and Higher Education of the Russian Federation, and project of the Ministry of Science and Higher Education of the Russian Federation No. 13.1902.21.0018. The authors thank the Associate Editor David Good and the reviewers for their assistance in the evaluation of this paper.

Competing interests. The authors declare none.

References

Barkov A., Martin R., Poirier G., Tarkian M., Pakhomovskii Y. and Men'shikov Y. (2000) Tatyanaite, a new Platinum-Group Mineral, the Pt analogue of taimyrite, from the Noril'sk Complex (Northern Siberia, Russia). *European Journal of Mineralogy*, **12**, 391–396.

Barnes S.J., Zientek M.L. and Severson M.J. (2011) Ni, Cu, Au and platinum-group element contents of sulphides associated with intraplate magmatism: a synthesis. *Canadian Journal of Earth Sciences*, **34**, 337–351.

Barnes S.J., Vaillant M.L., Godel B. and Lesher C.M. (2019) Droplets and bubbles: solidification of sulphide-rich vapour-saturated orthocumulates in the Norilsk-Talnakh Ni–Cu–PGE ore-bearing intrusions. *Journal of Petrology*, **60**, 269–300.

Begizov V.D., Meschankina V.I. and Dubakina L.S. (1974) Palladoarsenide Pd_2As – the new native palladium arsenide from the copper-Nickel Ores of Oktyabr'sky Deposit. *Zapiski Vsesoyuznogo Mineralogicheskogo Obshchestva*, **16**, 1294–1297 [in Russian].

Distler V.V. (1975) Zonality of copper-nickel ores of the Talnakh and Oktyabr'skoye deposits. *Geology of Ore Deposits*, **2**, 16–26.

Distler V.V., Genkin A.D., Filimonova A.A., Hitrov V.G. and Laputina I.P. (1975) The zoning of copper-nickel ores of Talnakh and Oktyabr'sky deposits. *Geology of Ore Deposits*, 2, 6–27 [in Russian].

Distler V.V., Smirnov A.V. and Grokhovskaya T.L. (1979) Stratification, latent layering of differentiated trap intrusions and conditions for the formation of sulfide mineralization. Pp. 211–292 in: *Conditions for the Formation of Magmatic Ore Deposits*. Nauka, Moscow, Russia [in Russian].

Distler V.V., Grokhovskaya T.L., Evstigneeva T.L., Sluzhenikin S.F., Filimonova A.A. and Dyuzhikov O.A. (1988) *Petrology of Magmatic Sulphide Ore Formation*. Nauka, Moscow, Russia [in Russian].

Distler V.V., Kulakov A.A., Sluzhenikin S.F. and Laputina I.P. (1996) Quenched sulphide solid solutions in Noril'sk ores. *Geology of Ore Deposits*, **38**, 41–53 [in Russian].

Distler V.V., Sluzhenikin S.F., Cabri L.J., Krivolutskaya N.A., Turovtsev D.M., Golovanova T.I., Mokhov A.V., Knauf V.V. and Oleshkevich O.I. (1999) The platinum ore of the Norilsk layered intrusions: The ratio of magmatic and fluid concentration of noble metals. *Geology of Ore Deposits*, **41**, 241–265 [in Russian].

Dodin D.A. and Batuev B.N. (1971) Geology and Petrology of the Talnakh Differentiated Intrusions and their Metamorphic Aureole. Pp. 31–100 in: *Petrology and Resource Potential of the Talnakh and Norilsk Differentiated Intrusions* (Urvantsev NN, editor). Nedra, Leningrad, Russia [in Russian].

Dodin D.A., Sluzhenikin S.F. and Bogomolov M.A. (2009) *Ores and Minerals of the Norilsk region*. Studio "Polyarnaya Zvezda", Moscow, Russia [in Russian].

Dyuzhikov O.A., Distler V.V., Strunin B.M., Mkrtychyan A.K., Sherman M.L. and Sluzhenikin S.F. (1992) *Geology and Metallogeny of Sulfide Deposits of Noril'sk Region USSR*. Society of Economic Geologists. Special Publication. 242 pp.

Egorova V.V. and Latypov R.M. (2013) Mafic-ultramafic sills: new insights from M- and S-shaped mineral and whole-rock compositional profiles. *Journal of Petrology*, **54**, 2155–2190.

Egorova V.V. and Shelepaev R.A. (2020) Reverse zoning in the marginal zones of layered ultramafic-mafic intrusions using the example of the Mazhalyk peridotite-gabbro massif (southeastern Tuva). *Geosphere Research*, **3**, 17–33 [in Russian].

Evstigneeva T.L. and Genkin A.D. (1983) Cabriite Pd_2SnCu, a new species in the mineral group of palladium, tin and copper compounds. *The Canadian Mineralogist*, **21**, 481–487.

Genkin A.D. (1968) *PGM and their associations in Cu-Ni ores of Noril'sk deposits*. Nauka, Moscow, Russia [in Russian].

Genkin A.D. and Evstigneeva T.L. (1986) Associations of platinum-group minerals of the Noril'sk copper-nickel sulphide ores. *Economic Geology*, **81**, 1203–1212.

Genkin A.D., Evstigneeva T.L., Troneva N.V. and Vyalsov N.L. (1969) Polarite Pd(Pb,B) - new mineral from copper-nickel sulfide ores. *Zapiski Vsesoyuznogo Mineralogicheskogo Obshchestva*, **6**, 708–715 [in Russian].

Genkin A.D., Kovalenker V.A., Smirnov A.V. and Muravitskaya G.N. (1977) Peculiarities of the mineral composition of Norilsk sulfide disseminated ores and their genetic characteristics. *Geology of Ore Deposits*, **1**, 24–35 [in Russian].

Genkin A.D., Distler V.V., Gladyshev G.D., Filimonova A.A., Evstigneeva T.L., Kovalenker V.A., Laputina I.P., Smirnov A.V. and Grokhovskaya T.L. (1981) *Sulphide Copper-Nickel Ores of the Noril'sk Deposits*. Nauka, Moscow, Russia [in Russian].

Godlevsky M.N. (1968) Magmatic deposits. Pp. 7–83 in *Genesis of Endogenous Ore Deposits*. Nedra, Moscow, Russia [in Russian].

Gorbachev N.S. (2006) Mineralogical and geochemical zoning and genesis of massive sulfide ores at the Oktyabr'sky deposit. *Geology of Ore Deposits*, **48**, 473–488.

Gorbachev N. and Nekrasov A.N. (2004) Layering of Fe-Ni-Cu sulfide melts: Experimental study and geological implications. *Doklady Earth Sciences*, **399**, 1256–1259.

Hall S.R. and Stewart J.M. (1973) The crystal structure of argentian pentlandite $(Fe,Ni)_8AgS_8$, compared with the refined structure of pentlandite $(Fe,Ni)_9S_8$. *The Canadian Mineralogist*, **12**, 169–177.

Kalugin V.M. and Latypov R.M. (2009) Theoretical modelling of zoning of massive sulfide ores in the ternary system Cu-Fe-S. Pp. 213–216 in: *The third international conference «Mafic-ultramafic complexes of folded regions and related deposits»*. Ekaterinburg, Russia [in Russian].

Kalugin V. and Latypov R. (2010) Two-stage formation of the Oktyabr'sky sulfide orebody, Noril'sk: evidence from vertical chemical zonation. *11th International Platinum Symposium*. Ontario Geological Survey, Miscellaneous Release-Data 269.

Kalugin V. and Latypov R. (2012) Top-down fractional crystallization of a sulfide liquid during formation of largest ore-body from the Noril'sk-Talnakh

https://doi.org/10.1180/mgm.2024.20 Published online by Cambridge University Press

PGE–Cu–Ni deposits, Russia. *Geophysical Research Abstracts*, **14**, EGU2012–4135.

Kaneda H., Takenouchi S. and Shoji T. (1986) Stability of pentlandite in the Fe–Ni–Co–S System. *Mineralium Deposita*, **21**, 169–180. https://doi.org/10.1007/BF00199797

Ketrov A., Yudovskaya M.A., Shelukhina Yu.S., Velivetskaya T.A. and Palamarchuk R.S. (2022) Sources and evolution of the sulfur isotope composition of sulfides of the Kharaelakh and Pyasino-Vologochansky intrusions (Norilsk ore district). *Geology of Ore Deposits*, **64**, 657–686 [in Russian].

Kitakaze A. (2008) Sugakiite, $Cu(Fe,Ni)_8S_8$, a new mineral from Hokkaido, Japan. *The Canadian Mineralogist*, **46**, 263–267.

Kolonin G.R., Orsoev D.A., Sinyakova E.F. and Kislov E.V. (2000) The use of Ni: Fe ratio in pentlandite for estimation of sulfur fugacity during the formation of PGE-bearing sulfide mineralization of Yoko-Dovyren. *Doklady Earth Sciences*, **370**, 87–91 [in Russian].

Komarova M.Z., Kozyrev S.M., Simonov O.N. and Lyul'ko V.A. (2002) The PGE mineralization of disseminated sulphide ores of the Noril'sk-Taimyr Region. Pp. 547–567 in: *Geology, Geochemistry, Mineralogy and Mineral Beneficiation of Platinum-Group Elements* (Cabri L.J., editor). **Vol. 54**. The Canadian Institute of Mining, Metallurgy and Petroleum. Montreal, Canada.

Korolyuk V.N., Usova L.V. and Nigmatulina E.N. (2009) On the accuracy of determining composition of principal rock-forming silicates and oxides with a Jeol JXA-8100 Electron Microprobe. *Journal of Analytical Chemistry*, **64**, 1070–1074.

Kosyakov V.I., Sinyakova E.F. and Shestakov V.A. (2003) The dependence of fugacity of sulphur from the composition of phase associations of Fe–FeS–NiS–Ni at 873 K. *Geochemistry International*, **7**, 730–740 [in Russian].

Kozyrev S.M., Komarova M.Z., Emelina L.N., Oleshkevich O.I., Yakovleva O.A., Lyalinov D.V. and Maximov V.I. (2002) The mineralogy and behaviour of PGM during processing of the Norilsk-Talnakh PGE-Cu-Ni ores. Pp. 757–791 in: *Geology, Geochemistry, Mineralogy and Mineral Beneficiation of Platinum-Group Elements* (Cabri L.J., editor). **Vol. 54**. The Canadian Institute of Mining, Metallurgy and Petroleum, Montreal, Canada.

Krivolutskaya N.A. (2014) *Evolution of Trap Magmatism and Processes Producing Pt-Cu-Ni Mineralization in the Noril'sk area*. KMK Scientific Press, Moscow, Russia [in Russian].

Krivolutskaya N., Nesterenko M., Gongalsky B., Korshunov D., Bychkova Y. and Svirskaya N (2018) Unique PGE-Cu-Ni Oktyabr'skoe Deposit (Noril'sk Area, Siberia, Russia): new data on its structure and mineralization. Pp. 253–255 in: *Proceedings of the 1st Springer Conference of the Arabian Journal of Geosciences (CAJG-1), Tunisia 2018*. https://doi.org/10.1007/978-3-030-01575-6_61 [Published in 2019].

Krivolutskaya N., Gongalsky B., Kedrovskaya T., Kubrakova I., Tyutyunnik O., Chikatueva V., Bychkova Y., Magazina L., Kovalchuk E., Yakushev A. and Kononkova N. (2019) Geology of the western flanks of the Oktyabr'skoe deposit, Noril'sk district, Russia: evidence of a closed magmatic system. *Mineralium Deposita*, **54**, 611–630.

Krivolutskaya N., Bychkova Y., Gongalsky B., Kubrakova I., Tyutyunnik O., Dekunova E. and Taskaev V. (2021) New geochemical and mineralogical data on rocks and ores of the NE flank of the Oktyabr'skoe deposit (Norilsk area) and a view on their origin. *Minerals*, **11**, 44.

Kunilov V.Ye. (1994) Geology of the Noril'sk region: the history of the discovery, prospecting, exploration and mining of the Noril'sk Deposits. *Proceedings of the Sudbury-Noril'sk Symposium* (Lightfoot P.C. and Naldrett A.J., editors). Special Publication 5. Geological Survey, Ontario.

Latypov R.M. and Egorova V.V. (2012) Plagioclase compositions give evidence for in situ crystallization under horizontal flow conditions in mafic sills. *Geology*, **40**, 883–886.

Latypov R.M., Chistyakova S.Yu. and Alapieti T.T. (2007) Revisiting the problem of chilled margins associated with marginal reversals in mafic-ultramafic intrusive bodies. *Lithos*, **99**, 178–206.

Latypov R.M., Hanski E., Lavrenchuk A., Huhma H. and Havela T. (2011) A "three-increase model" for origin of marginal reversal in the Koitelainen layered intrusion, Finland. *Journal of Petrology*, **52**, 733–764.

Likhachev A.P. (1973) On the nature of magmatic deposits. *Soviet Geology*, **5**, 33–47 [in Russian].

Likhachev A.P. (1994) Ore-bearing intrusions of the Noril'sk Region. Pp 185–201 in: *Proceedings of the Sudbury-Noril'sk Symposium* (Lightfoot P.C. and Naldrett A.J., editors). Special Publication 5. Geological Survey, Ontario.

Likhachev A.P. (1996) About dynamics of the formation of Talnakh ore-bearing intrusion and related Pt-Cu-Ni deposits. *Otechestvennaya Geologiya*, **8**, 20–26 [in Russian].

Likhachev A.P. (2004) On the possibility of platinum-copper-nickel ore formation in impact structures. *Domestic Geology*, **6**, 3–12 [in Russian].

Likhachev A.P. (2006) *Platinum-Copper-Nickel Deposits*. Elan, Moscow, Russia [in Russian].

Likhachev A.P. and Kukoev V.A. (1973) On melting and phase relations in sulfide, silicate and sulfide-silicate systems. *Geology of Ore Deposits*, **5**, 32–45 [in Russian].

Lul'ko V.A., Fedorenko V.A., Distler V.V. and Sluzhenikin S.F. (1994) Geology and ore deposits of the Norilsk region. P. 67 in: *Guidebook of VII International Platinum Symposium*. Moscovsky contact Press, Moscow, Russia.

Malich K.N., Belousova E., Griffin W., Badanina I., Pearson N., Presnyakov S., Tuganova E. (2010) Magmatic evolution of the ultramafic-mafic Kharaelakh intrusion (Siberian Craton, Russia): insights from trace-element, U-Pb and Hf-isotope data on zircon. *Contributions to Mineralogy and Petrology*, **159**, 753–768.

Melfos V., Vavelidis M. and Arikas K. (2001) A new occurrence of argentopentlandite and gold from the Au-Ag-rich copper mineralisation in the Paliomylos area, Serbomacedonian massif, Central Macedonia, Greece. *Bulletin of the Geological Society of Greece*, **34**, 1065–1072.

Naldrett A.J. (2004) *Magmatic Sulphide Deposits: Geology, Geochemistry and Exploration*. Springer, Berlin, Heidelberg, 728 p.

Naldrett A.J., Asif M., Gorbachev N.S., Kunilov V.Ye., Stekhin A.I., Fedorenko V.A. and Lightfoot P.C. (1994) The Composition of the Ni-Cu Ores of the Oktyabr'sky Deposit, Noril'sk Region. Pp. 357–372 in: *Proceedings of the Sudbury-Noril'sk Symposium* (Lightfoot P.C. and Naldrett A.J., editors). Special Publication 5. Geological Survey, Ontario.

Naldrett A.J., Fedorenko V.A., Lightfoot P.C., Kunilov V.E., Gorbachev N.S., Doherty W. and Johan Z. (1995) Ni-Cu-PGE deposits of the Noril'sk region, Siberia: their formation in conduits for flood basalt volcanism. *Institute if Mining and Metallurgy*, **104**, B18–B36.

Naldrett A.J., Fedorenko V., Shushen L., Asif M., Kunilov V.E., Stekhin A.I., Lightfoot P.C. and Gorbachev N.S. (1996) Controls on the composition of Ni-Cu sulsulfide deposits as illustrated by those at Noril'sk, Siberia. *Economic Geology*, **91**, 751–773.

Peregoedova A.V. (1999) *Physical and chemical behavior of Pt and Pd during crystallization of Fe, Ni, Cu-containing sulphide melts, and in subsequent subsolidus transformations*. Author. Dis. of kand. geol.-min. nauk, Novosibirsk [in Russian].

Rad'ko V.A. (1991) Model of dynamic differentiation of intrusive traps in the north-west of the Siberian Platform. *Geology and Geophysics*, **11**, 19–27 [in Russian].

Razin L.V., Dubakina L.S. and Dubinchuk V.T. (1976) Rhombic stannide of palladium, copper and platinum from copper-nickel sulfide ores of Norilsk-type deposits. *Zapiski Vsesoyuznogo Mineralogicheskogo Obshchestva*, **105**, 206–213 [in Russian].

Rudashevskii N.S., Mintkenov G.A., Karpenkov A.M. and Shiskin N.N. (1977) Silver-containing pentlandite — the independent mineral species argentopentlandite. *Zapiski Vsesoyuznogo Mineralogicheskogo Obshchestva*, **106**, 688–691 [in Russian].

Sinyakova E.F., Borisenko A.S., Karmanov N.S. and Kosyakov V.I. (2019) Behavior of noble metals during fractional crystallization of Cu–Fe–Ni–(Pt, Pd, Rh, Ir, Ru, Ag, Au, Te) sulfide melts. *Russian Geology and Geophysics*, **60**, 642– 661.

Sluzhenikin S.F. (2010) Platinum-copper-nickel and platinum ores of the Norilsk region and their ore mineralization. *Russian Chemical Journal*, **LIV2**, 38–49 [in Russian].

Sluzhenikin S.F. (2011) Platinum-copper-nickel and platinum ores of Noril'sk region and their ore mineralization. *Russian Journal of General Chemistry*, **81**, 1288–1301.

Sluzhenikin S.F. and Mokhov A.V. (2014) Gold and silver in PGE-Cu-Ni and PGE ores of the Noril'sk deposits, Russia. *Mineralium Deposita*, **50**. https://doi.org/10.1007/s00126-014-0543-2

https://doi.org/10.1180/mgm.2024.20 Published online by Cambridge University Press

Spiridonov E.M. (2010) Ore-magmatic systems of the Noril'sk ore field. *Russian Geology and Geophysics*, **51**, 1059–1077. https://doi.org/10.1016/j.rgg.2010.08.011

Spiridonov E.M., Kulagov E.A.and Kulikova I.M. (2003) Pt-Pd tetraauricupride and associated minerals in ores of the Norilsk-I deposit. *Geology of Ore Deposits*, **45**, 232–241.

Spiridonov E.M., Kulagov E.A. and Kulikova I.M. (2004) Palladium, platinum and gold mineral assemblages in ores of the Norilsk deposit. *Geologe of Ore Deposit*, **46**, 150–166.

Spiridonov E.M., Kulagov E.A., Serova AA., Kulikova I.M., Korotaeva N.N., Sereda E.V., Tushentsova I.N., Belyakov S.N. and Zhukov N.N. (2015) Genetic Pd, Pt, Au, Ag, and Rh mineralogy in Noril'sk sulfide ores. *Geology of Ore Deposits*, **57**, 402–432. https://doi.org/10.1134/S1075701515050062

Stekhin A.I. (1994) Mineralogical and chemical characteristics of the Cu-Ni ores of the Oktyabr'sky and Talnakh deposits. Pp. 217–230 in *Proceedings of the Sudbury-Noril'sk Symposium* (Lightfoot P.C. and Naldrett A.J., editors). Special Publication 5. Geological Survey, Ontario.

Strunin B.M. (editor) (1994) *Explanatory Notes to 1:200000 Geological Map of the Noril'sk Mining District*. St. Petersburg, VSEGEI [in Russian].

Tolstykh N.D., Shvedov G.I., Polonyankin A.A. and Zemlyanssky S.A. (2017) Mineralogical and geochemical feature of the disseminated ores of the southern part of the Noril'sk 1 deposit. *IOP Conf Series: Earth and Environmental Science*, **110**, 012021. https://doi.org/10.1088/1755-1315/110/1/012021

Tolstykh N., Krivolutskaya N., Safonova I., Shapovalova M., Zhitova L. and Abersteinerd A. (2020a) Unique cu-rich sulphide ores of the southern-2 orebody in the Talnakh intrusion, Noril'sk area (Russia): geochemistry, mineralogy and conditions of crystallization. *Ore Geology Reviews*, **122**, 103525.

Tolstykh N., Shvedov G., Polonyankin A. and Korolyuk V. (2020b) Geochemical features and mineral associations of differentiated rocks of the Norilsk 1 intrusion. *Minerals*, **10**, 688. https://doi.org/10.3390/min10080688

Tolstykh N., Garcia J. and Shvedov G. (2021) Distribution of sulfides and PGE minerals in the picritic and taxitic gabbro-dolerites of the Norilsk 1 intrusion. *The Canadian Mineralogist*, **59**, 1437–1451. https://doi.org/10.3749/canmin.2100037

Torgashin A.S. (1994) Geology of the massive and copper ores of the western part of the Oktyabr'sky Deposit. *Sudbury–Noril'sk Symposium, Ontario Geological Survey Special Paper*, **5**, 231–241.

Turovtsev D.M. (2002) *Contact Metamorphism of Norilsk Intrusions*. Mir, Moscow, Russia, 318 pp. [in Russian].

Valetov A.V., Badtiev B.P. and Ryabikin V.A. (2000) Present-day state of resource base of the Noril'sk Mining Company. *Tsvetn Metally*, **6**, 10–14 [in Russian].

Vaughan D.J. and Craig J.R. (1981) *Mineral Chemistry of Metal Sulphides*. Nauchnyy Mir, Moscow, Russia [in Russian].

Yao Z., Mungall J.E. and Qin K.A. (2019) Preliminary model for the migration of sulfide droplets in a magmatic conduit and the significance of volatiles. *Journal of Petrology*, **60**, 2281–2315.

Zientek M.L. and Likhachev A.P. (1992) Compositional constraints on the genesis of ore deposits of the Noril'sk-Talnakh distrtct' Siberia. *The Canadian Mineralogist*, **30**, 492 [Abstracts of the Sudbury-Noril'sk symposium].

Zientek M.L., Likhachev A.P., Kunilov V.E., Barnes S.-J., Meier A.L., Carlson R.R., Briggs P.H., Fries T.L. and Adrian B.M. (1994) Cumulus processes and the composition of magmatic ore deposits: examples from the Talnakh district, Russia. Pp. 373–392 in: *Proceedings of the Sudbury-Noril'sk Symposium* (Lightfoot P.C. and Naldrett A.J., editors). Special Publication 5. Geological Survey, Ontario.

Zolotukhin V.V. (1964) Reaction aggregates in the Norilsk ores and the problem of disseminated sulfide mineralization in gabbro-dolerites. *Doklady Academy of Sciences USSR*, **154**, 600–603 [in Russian].

Zolotukhin V.V., Ryabov V.V., Vasil'ev Y.R. and Shatkov B.A. (1975) *Petrology of the Talnakh Differentiated Ore-Bearing Trap Intrusion*. Nauka, Novosibirsk, Russia [in Russian].

https://doi.org/10.1180/mgm.2024.20 Published online by Cambridge University Press